Xcr1^{+} type 1 conventional dendritic cells are essential mediators for atherosclerosis progression

Running tittle: Targeting of cDC1 cells attenuates atherosclerosis

Tianhan Li[1#], Liaoxun Lu[2#], Juanjuan Qiu[2], Xin Dong[2], Le Yang[2], Kexin He[2], Yanrong Gu[2], Binhui Zhou[2], Tingting Jia[2], Toby Lawrence[3], Marie Malissen[3], Guixue Wang[4], Rong Huang[2], Hui Wang[2], Bernard Malissen[3*], Yinming Liang[2,5*] Lichen Zhang[2*]

[1]*School of Basic Medicine, Xinxiang Medical University, Xinxiang, China.*

[2]*School of Medical Technology, Xinxiang Medical University, Xinxiang, China.*

[3]*Centre d'Immunologie de Marseille-Luminy, INSERM, CNRS, Aix-Marseille Université, Marseille, France*

[4]*Key Laboratory for Biorheological Science and Technology of Ministry of Education, State and Local Joint Engineering Laboratory for Vascular Implants, Bioengineering College of Chongqing University, Chongqing, China*

[5]*Center of Disease Model and Immunology, Hunan Academy of Chinese Medicine, Changsha, China.*

[#]*These authors contributed equally to this work.*

[*]Correspondence: yinming.liang@gris.org.cn (Y L); zhanglichen@gris.org.cn (L Z).

bernardm@ciml.univ-mrs.fr (B M).

Abstract:

Background:

Atherosclerosis is characterized by lipid accumulation within plaques, leading to foam cell

formation and an inflammatory response within the aortic lesions. Lipid disorders have been extensively investigated, however the cellular and molecular mechanisms that trigger the inflammatory response in atherosclerotic plaques remain far from being fully understood. Xcr1^{+} cDC1 cells are newly identified antigen-presenting cells in activating immune cells. However, the role of cDC1 cells in the development of atherosclerosis remains highly controversial.

Results:

We first confirmed the presence of cDC1 within human atherosclerotic plaques and discovered a significant association between the increasing cDC1 numbers and atherosclerosis progression in mice. Subsequently, we established Xcr1$^{Cre\text{-}Gfp}$ Rosa26$^{LSL\text{-}DTA}$ ApoE$^{-/-}$ mice, a novel and complex genetic model, in which cDC1 was constitutively depleted *in vivo* during atherosclerosis development. Intriguingly, we observed a notable reduction in atherosclerotic lesions in hyperlipidemic mice, alongside suppressed T cell activation of both CD4^{+} and CD8^{+} subsets in the aortic plaques. Notably, aortic macrophages and serum lipid levels were not significantly changed in the cDC1-depleted mice. Single-cell RNA sequencing revealed heterogeneity of Xcr1^{+} cDC1 cells across the aorta and lymphoid organs under hyperlipidemic conditions. As Xcr1 is the sole receptor for Xcl1, we next explored to target Xcr1^{+} cDC1 cells via Xcl1 by establishing Xcl1 and ApoE deficient mice. Xcl1 knockout mice exhibited decreased atherosclerotic plaque formation and reduced aortic cDC1 accumulation, indicating that Xcl1 contributes to cDC1-mediated atherosclerotic lesion development.

Conclusions:

Our results reveal crucial roles of cDC1 in atherosclerosis progression and provide insights into the development of immunotherapies by targeting cDC1 through Xcl1.

45 **Introduction**

46 Atherosclerosis is a chronic inflammatory disease that affects the large and medium-sized arteries,
47 and it is the leading cause of cardiovascular mortality and morbidity worldwide [1]. Atherosclerosis
48 is a complex pathological process during which lipid-laden phagocytes such as macrophages, along
49 with lymphocytes and dendritic cells, accumulate in the plaque [2]. Mounting evidence from animal
50 models and human studies demonstrates involvement of both the innate and adaptive immunity in
51 the development of atherosclerosis [3-5]. In healthy arteries, DCs are typically present in the
52 subendothelial space and work in the front line of immune surveillance [6, 7], and small portion of
53 resident vascular DCs are localized in the adventitia. Various studies have demonstrated that DCs
54 accumulated in the advanced atherosclerotic lesions in both humans and animal models [8-11].
55 Recently, several phenotypically and functionally distinct vascular DCs have been identified in
56 mouse and human atherosclerotic lesions [12]. Xcr1^{+} type 1 conventional dendritic cells (Xcr1^{+}
57 cDC1) (also known as CD8^{+} DC or CD103^{+} DCs) has been recognized for its role in cross-
58 presentation and activating naive CD8^{+} T cells, and are critical for anti-viral and anti-tumor immune
59 responses [13, 14]. Owing to the challenges associated with obtaining a model for specific cDC1
60 depletion *in vivo*, previous studies investigating the role of cDC1 cells in atherosclerosis using
61 various knockout mice have produced conflicting results [15-19]. It is important to note that
62 previous Cre lines developed to achieve specific Cre expression in cDC1s still led to leakiness in
63 recombinase activity outside of cDC1s, as demonstrated in previous publications [20, 21]. Moreover,
64 scant mechanistic understanding regarding the regulation of cDC1 activity during atherosclerosis
65 has been reported. Therefore, developing a more specific mouse model for cDC1 is essential for
66 elucidating its precise role in atherosclerosis. Here, we established a novel Cre line Xcr1$^{Cre\text{-}Gfp}$ mice

and did not observe any leakiness of Cre activity, and further experiments revealed that specific depletion cDC1 attenuates atherosclerosis development by inhibiting both $CD4^+$ and $CD8^+$ T cell activation in hyperlipidemic $Xcr1^{Cre\text{-}Gfp}$ $Rosa26^{LSL\text{-}DTA}$ $ApoE^{-/-}$ mice.

The origin of phagocytes within the atherosclerotic plaques has been controversial. Studies have shown that the major contribution of macrophages in the aortic plaque is recruited from the circulation, while other studies have emphasized the significance of local proliferation [22, 23]. Tissue-resident dendritic cells inside the plaques have been well documented [24, 25], regardless of the fact that the contribution and origin of $Xcr1^+$ cDC1 have not been appropriately addressed. To understand the origin of $Xcr1^+$ cDC1 inside the plaque, we performed bone marrow transplantation using $Xcr1^{Cre\text{-}Gfp}$ $Rosa26^{LSL\text{-}DTA}$ mice as donors and found that in $ApoE^{-/-}$ recipient mice placed on a high-fat diet (HFD), cDC1 cells were completely absent in the aortas. Therefore, our experiments have elucidated that cDC1 cells in the atherosclerotic plaques originate from the bone marrow. Further single cell RNA sequencing illustrated that notable differences in $Xcr1^+$ cDC1 cells are discovered among the aorta, spleen, and lymph nodes. *Ccr2*, *Sept3* and *Cldnd1* were highly expressed in $Xcr1^+$ cDC1 cells from aorta compared with that from spleen and lymph nodes.

We further aimed to ascertain whether cDC1 can be modulated by targeting the chemokine Xcl1, which is a ligand of Xcr1. Considering the vital role that $Xcr1^+$ cDC1 plays in the progression of atherosclerosis and the therapeutic potential of manipulating their functions via chemokines[26], comprehending the feasibility of targeting Xcl1 holds considerable promise for developing novel therapeutic approaches to halt the advancement of atherosclerosis. We conducted further studies using $Xcl1^{-/-}$ $ApoE^{-/-}$ double knockout mice to assess the pathological grade of atherosclerotic lesions. Our data indicated that the knockout of Xcl1 led to a mild yet significant reduction of cDC1

89 cells in the aorta. However, strikingly, when compared to the ApoE$^{-/-}$ control mice, the Xcl1$^{-/-}$
90 ApoE$^{-/-}$ mice exhibited a markedly decreased severity of the atherosclerotic lesions, to an extent
91 comparable to that observed in cDC1-depleted Xcr1$^{Cre\text{-}Gfp}$ Rosa26$^{LSL\text{-}DTA}$ ApoE$^{-/-}$ mice.
92 Therefore, our study which employed genetic models to deplete Xcr1^{+} cDC1 *in vivo* in
93 hyperlipidemic mice, has unequivocally determined the essential role of this specific cell type in the
94 development of atherosclerosis. Besides their well-established role in cross-presentation to CD8^{+} T
95 cells, recent studies have shown Xcr1^{+} cDC1 cells also engage with CD4^{+} T cells to augment CD8^{+}
96 T cell responses [20, 27]. Our data showing Xcr1^{+} cDC1-dependent CD4 and CD8 T cell activation
97 in atherosclerotic plaques is in line with the new paradigm for cDC1s as a platform for both CD4
98 and CD8 T cell responses in the novel context of atherosclerosis.
99 Most importantly, we have successfully demonstrated that targeting the chemokine Xcl1, the ligand
100 of Xcr1, can effectively inhibit atherosclerosis. These novel findings hold the potential to forge a
101 novel trajectory for therapeutic interventions within the field of atherosclerosis, presenting
102 promising prospects for better understanding and treatment of this disorder.
103

104 ## Results:

105 **Progressive accumulation of Xcr1^{+} cDC1 cells in advanced atherosclerotic lesions in human**
106 **and mice**

107 Dendritic cells are present in healthy arteries and accumulate within atherosclerotic lesions,
108 participating in various pathogenic and protective mechanisms during atherogenesis [28, 29].
109 However, the intra-plaque dynamics of cDC1 and their contribution to atherosclerosis remain

110 undetermined. Using the archived specimens of paraffin-embedded human atherosclerotic arteries
111 from our previous study [30], we examined the Xcr1^{+} dendritic cells in human atherosclerotic
112 plaques. As shown in **Figure 1A and 1B**, Xcr1^{+} dendritic cells were significantly more abundant in
113 the plaque area of the human femoral artery compared to that in the plaque-free area. Similarly, the
114 immunofluorescence staining results using specific antibodies for Xcr1 and CD11c revealed that
115 Xcr1^{+}CD11c^{+} dendritic cells accumulated in the plaques of the aortic root in ApoE$^{-/-}$ mice that were
116 placed on a HFD for 16 weeks (**Figure 1C and 1D**). Sample preparations entailed sectioning and
117 appropriate fixation of the aortic root tissues, which were described in greater detail in the Methods
118 and Materials section. To further elucidate the dynamics of Xcr1^{+} cDC1 cells within the plaque
119 during the progression of atherosclerosis, we carried out immunohistochemical analyses of these
120 cells in the lesioned aortic root (**Figure 1E**). The area positive for Xcr1 expression was quantified
121 at 8-week on a normal diet (ND), 8-week on HFD, 12-week on HFD and 16-week on HFD,
122 respectively. Quantitative analysis was conducted using image processing software, revealing a
123 continuous accumulation of Xcr1^{+} cDC1 cells in the lesioned area as the disease progressed (**Figure**
124 **1F**). Therefore, our experiments provided data indicating the enrichment of Xcr1^{+} cDC1 cells in
125 aortic lesions in both humans and mice, and demonstrated that the accumulation of Xcr1^{+} cDC1
126 cells was significantly greater during the progression of atherosclerosis.

127 **Xcr1$^{Cre\text{-}Gfp}$ is selectively expressed in cDC1**

128 To understand the role of Xcr1^{+} cDC1 in regulating the development of atherosclerosis, we
129 established the Xcr1$^{Cre\text{-}Gfp}$ ApoE$^{-/-}$ mice in which the Cre recombinase and eGFP was co-expressed
130 under the control of endogenous Xcr1 promoter following start codon (**Figure S1**). This new Cre
131 line differs from a previous design in which Cre recombinase was expressed via IRES linkage at the

132 3' UTR and leaked expression of Cre was frequently observed [20, 31]. To verify the fidelity of Cre
133 expression under hyperlipidemic condition, we used hyperlipidemic ApoE$^{-/-}$ mice as recipient mice
134 and used bone marrow cells from Xcr1$^{Cre\text{-}Gfp}$ Rosa26$^{LSL\text{-}tdRFP}$ mice as donors for the bone marrow
135 transplantation (**Figure 2A**). In Xcr1$^{Cre\text{-}Gfp}$ Rosa26$^{LSL\text{-}tdRFP}$ mice, the presence of Cre protein would
136 turn on the expression of tdRFP as a reporter for the activity of Cre recombinase [32]. Remarkably,
137 we found that the expression of tdRFP was exclusively present in Xcr1^{+} cDC1 when mice were fed
138 a HFD for 16 weeks in the bone marrow transplanted mice, and the Cre recombinase activity was
139 not detectable in non-cDC1 cells (**Figure 2B and 2C**).
140 To determine the specificity of GFP expression originating from Xcr1$^{Cre\text{-}Gfp}$ genetic modification,
141 we examined the GFP levels in three populations of DCs, namely pDC, cDC1, and cDC2 cells, from
142 the spleen of Xcr1$^{Cre\text{-}Gfp}$ ApoE$^{-/-}$ mice that were fed a HFD for 16 weeks. As expected, we found
143 that the GFP expression was stringently restricted to cDC1 cells (**Figure 2D and 2E**). In parallel,
144 we compared the GFP expression in Xcr1^{+} cDC1-depleted mice that were fed a HFD for 16 weeks.
145 Such cDC1-depleted Xcr1$^{Cre\text{-}Gfp}$ Rosa26$^{LSL\text{-}DTA}$ ApoE$^{-/-}$ mice were obtained by crossing Xcr1$^{Cre\text{-}Gfp}$
146 ApoE$^{-/-}$ mice with Rosa26$^{LSL\text{-}DTA}$ ApoE$^{-/-}$ mice. Strikingly, we observed a complete loss of GFP-
147 positive cells and Xcr1^{+} cDC1 cells in Xcr1^{+} cDC1-depleted mice (**Figure 2D and 2F**). We also
148 examined DCs, including pDCs, cDC1, and cDC2, in the lymph nodes and spleens of Xcr1$^{Cre\text{-}Gfp}$
149 Rosa26$^{LSL\text{-}DTA}$ ApoE$^{-/-}$ and ApoE$^{-/-}$ mice maintained on a ND for 7 weeks. The flow cytometric
150 analyses also confirmed the absence of Xcr1^{+} cDC1 population in Xcr1$^{Cre\text{-}Gfp}$ Rosa26$^{LSL\text{-}DTA}$ ApoE^{-}
151 $^{/-}$ mice (**Figure S2**). Collectively, these data suggest that Cre recombinase activity was selectively
152 confined to cDC1 cells, and no leakiness was observed in lineages other than the Xcr1^{+} cDC1
153 population. We also demonstrated that Xcr1$^{Cre\text{-}Gfp}$ Rosa26$^{LSL\text{-}DTA}$ ApoE$^{-/-}$ mice constitute a desirable

model for exploring the role of cDC1 in atherosclerosis.

The specific depletion of Xcr1^{+} cDC1 cells significantly alleviates atherosclerosis without influencing the lipid profile and the number of intra-plaque macrophages

To investigate the role of cDC1 cells in atherosclerosis, both Xcr1$^{Cre\text{-}Gfp}$ Rosa26$^{LSL\text{-}DTA}$ ApoE$^{-/-}$ and the control ApoE$^{-/-}$ mice were subjected to a HFD for 16 weeks. The ORO staining results demonstrated that the size of lesion in both descending aorta and aortic root was significantly smaller in Xcr1$^{Cre\text{-}Gfp}$ Rosa26$^{LSL\text{-}DTA}$ ApoE$^{-/-}$ mice compared with ApoE$^{-/-}$ control mice (12.82% *vs* 6.01% in descending aorta; 39.25% *vs* 33.57% in ORO-stained aortic root) (**Figure 3A-D**). Given that macrophages play a pivotal role in the development and progression of atherosclerotic lesions, particularly within the necrotic core [33, 34], we next investigated macrophage involvement in the aorta using IHC and flow cytometry. Interestingly, no significant differences were observed in the necrotic core area of the aortic root between Xcr1$^{Cre\text{-}Gfp}$ Rosa26$^{LSL\text{-}DTA}$ ApoE$^{-/-}$ mice and ApoE$^{-/-}$ control mice (**Figure 3E and 3F**). Similarly, subsequent flow cytometry analyses and IHC results revealed comparable proportions of F4/80^{+} CD11b^{+} macrophages in the aorta, as well as similar percentages of CD68-positive macrophages in the aortic lesions between the two groups of mice (**Figure 3G-J**). Furthermore, since dyslipidemia is a key characteristic of HFD-treated ApoE$^{-/-}$ mice [35, 36], it is critical to assess body weight and lipid profiles in both groups. Our results indicated no significant differences in body weight or levels of total cholesterol (TC), triglycerides (TG), low-density lipoprotein (LDL), and high-density lipoprotein (HDL) between the two groups (**Figure S3A-B**). Additionally, ORO staining of the liver revealed no significant differences either (**Figure S3C-D**). Taken together, these results suggested that specific depletion of cDC1 attenuated atherogenesis without affecting lipid status or macrophagic accumulation in aortic lesions.

176 **Specific depletion of cDC1 attenuates the development of atherosclerosis by modulating the**
177 **activation of T cell in ApoE$^{-/-}$ mice**

178 T cells are among the critical drivers of the pathogenesis of atherosclerosis, and therefore, the
179 triggers of T cell activation in aortic plaques are of great interest for controlling disease progression
180 [2, 37, 38]. We initially analyzed the cDC1 cells through flow cytometry in both Xcr1^{+} cDC1
181 depleted mice and control mice. In the Xcr1$^{Cre\text{-}Gfp}$ Rosa26$^{LSL\text{-}DTA}$ ApoE$^{-/-}$ mice that were fed a HFD
182 for 16 weeks, we observed a total absence of Xcr1^{+} cDC1 in the aorta, lymph nodes, and spleen
183 (**Figure 4A-C and Figure S4**). Subsequently, we assessed T cell phenotype in the two groups of
184 mice. While neither the frequencies nor absolute counts of aortic CD4^{+} and CD8^{+} T cells differed
185 significantly between two groups of mice (**Figure 4D-F**), CD69 frequency and CD44 MFI (Mean
186 Fluorescence Intensity), the T cell activation markers, were significantly reduced in both CD4^{+} and
187 CD8^{+} T cells from Xcr1^{+} cDC1 depleted mice compared to controls (**Figure 4G** and **H**).
188 Interestingly, such decreased frequencies of CD69^{+} T cells were only observed in aortic lesions but
189 not in lymphoid organs such as lymph nodes and the spleen in the Xcr1^{+} cDC1 depleted mice
190 (**Figure S5A-B and S5D-E**). We further analyzed the absolute numbers of CD8^{+} and CD4^{+} T cells
191 in the spleen and lymph nodes and found that the absolute numbers of CD8^{+} and CD4^{+} T cells were
192 markedly reduced in the spleen but not in the lymph nodes in Xcr1$^{Cre\text{-}Gfp}$ Rosa26$^{LSL\text{-}DTA}$ ApoE$^{-/-}$
193 mice compared to those in ApoE$^{-/-}$ mice (**Figure S5C and S5F**). Absence of cDC1 also resulted in
194 reduced frequencies of CD8^{+} T cells in both spleen and lymph nodes in hyperlipidemic mice. We
195 also analyzed T cell populations in the lymph nodes and spleen in two groups of mice that were fed
196 a ND and found that the frequencies of CD8^{+} T cells were significantly decreased in the lymph
197 nodes of Xcr1^{+} cDC1 depleted mice (**Figure S6A-B**). More importantly, the frequencies of CD44^{high}

198 CD62L^{low} activated memory cells within the CD8^{+} subsets in both the spleen and lymph nodes were
199 significantly lower than those in the ApoE$^{-/-}$ control mice (**Figure S6A-D**). However, in the CD4^{+}
200 subsets, such frequencies of CD44^{high} CD62L^{low} activated cells were comparable in the lymph nodes
201 but marginally lower in the spleen (**Figure S6A-D**). It is important to note that the decreased
202 absolute number of CD8^{+} T cells in the spleen in Xcr1^{+} cDC1 depleted mice was only observed in
203 HFD groups but not in ND groups (**Figure S5F and Figure S6F**). Our data indicate that in aortic
204 plaques, Xcr1^{+} cDC1 cells are implicated in activating CD4^{+} and CD8^{+} T cells, and the loss of the
205 cDC1 population led to a decreased absolute count of CD8^{+} T cells in the lymph nodes of HFD
206 treated mice. Whereas in mice treated with a ND, the loss of the cDC1 population resulted in reduced
207 frequencies of activated memory T cells but did not affect the absolute counts of T cells. Attenuated
208 T cell activation might account for the mitigated atherosclerosis in Xcr1^{+} cDC1 depleted mice.

209 **Characterization of aortic Xcr1^{+} cDC1 cells in atherosclerotic lesions**

210 Although the majority of cDC1 cells derive from bone marrow, other mechanisms such as local
211 proliferation of existing DCs can also contribute to the cDC1 population in inflammatory diseases
212 [39, 40]. It remains unclear whether cDC1 cells in lymphoid organs such as spleen and lymph nodes
213 represent a different status compared to cDC1 cells in atherosclerotic lesions. To elucidate the source
214 and status of Xcr1^{+} cDC1 in atherosclerotic lesions, we performed bone marrow transplantation and
215 single-cell RNA sequencing (sc-RNA seq) of cDC1 cells from aortic plaques and lymphoid organs.
216 We conducted bone marrow transplantation using Xcr1$^{Cre\text{-}Gfp}$ Rosa26$^{LSL\text{-}DTA}$ or WT mice that carry
217 the CD45.2 congenic markers as donors, and CD45.1^{+} CD45.2^{+} ApoE$^{-/-}$ mice as recipients (**Figure**
218 **S7A**). Our data showed that body weight, lipid profile, and hepatic lipid accumulation were
219 comparable between two groups of bone marrow transplanted mice after being fed with a HFD for

220 16 weeks (**Figure S7B-D**). Interestingly, flow cytometric analysis of the aorta displayed almost
221 complete depletion of cDC1 cells in ApoE$^{-/-}$ recipient mice transplanted with Xcr1$^{Cre\text{-}Gfp}$ Rosa26$^{LSL\text{-}}$
222 ^{DTA} bone marrow mice (**Figure S7E**). Strikingly we did not find observe significant changes in
223 pDCs and CD64^{+}F4/80^{+} aortic macrophages (**Figure S7E-F**). Therefore, our bone marrow
224 transplantation experiments further confirmed fidelity of the Cre recombinase expression in cDC1
225 cells in mice.
226 Next, we carried out sc-RNA seq to characterize Xcr1^{+} cDC1 cells from multiple organs of
227 hyperlipidemic mice. Due to the scarcity of Xcr1^{+} cDC1 cells that can be sorted by FACS and
228 processed for sc-RNA seq, we pooled FACS sorted Xcr1^{+} cDC1 cells from three organs of
229 hyperlipidemic ApoE-deficient mice fed a HFD for 20 weeks, including the aorta, spleen, and lymph
230 nodes, and Xcr1^{+} cDC1 cells from aorta and splenocytes of ApoE-deficient mice fed a ND. Libraries
231 for sc-RNA seq were prepared using barcode oligos conjugated to anti-CD45 antibodies for surface
232 staining so that samples from each type of organ could be compared in sequential analyses.
233 Therefore, we had a total of five samples, and our focus was to understand the differences between
234 Xcr1^{+} cDC1 cells from three different organs under hyperlipidemic conditions. The cells were sorted
235 by gating Xcr1-positive cells out of the MHCII^{+}CD11c^{+} conventional dendritic cells (**Figure S8**).
236 Firstly, we obtained the UMAP plot of 10 clusters of cDC1 cells using the Seurat 4.0 package
237 (**Figure 5A**). In this analysis, 3830 quality-controlled Xcr1^{+} cDC1 cells were from three types of
238 organs in hyperlipidemic mice, and an additional 2081 cells were from cDC1 cells sorted from the
239 spleen and aorta of ApoE deficient mice fed on a ND. The clusters were differentiated according to
240 top 10 differentially expressed genes (**Supplementary Table 1**), and the heatmap shows marker
241 genes and heterogeneity among the 10 clusters of cDC1 cells (**Figure 5B**). The purpose of this

experiment was to determine whether cDC1 cells from different organs possess unique features and whether cDC1 cells from aortic lesions can be characterized by the expression of marker genes. In hyperlipidemic mice, cDC1 cells from the spleen and lymph nodes differed quite dramatically in Cluster 2 (*Stk17b* and *Gpr171* highly expressing cells), where 28.9% of cDC1 cells from the spleen versus 1.0% of cDC1 cells from the lymph nodes were located. Conversely, 3.15% of cDC1 cells from the spleen versus 32.4% of cDC1 cells from the lymph nodes fell in Cluster 3 (*Ccl5* and *Epsti1* highly expressing cells), and 4.6% of cDC1 cells from the spleen versus 25.9% of cDC1 cells from the lymph nodes fell in Cluster 4 (*Slfn5* and *Ifi44* highly expressing cells). Despite the fact that we had only transcriptomic data for 68 Xcr1$^+$ cDC1 cells from aortic lesions, we were surprised to find that such aortic cDC1 mainly fell into Cluster 1, 4 and 5, comprising 80.8% of the cells analyzed (**Figure 5C**). In Cluster 1 (*Hspa1b* and *Dnajb1* highly expressing cells), where aortic cDC1 is dominantly enriched, the cDC1 cells sorted from lymph nodes were essentially absent, while in Cluster 4, aortic cDC1 cells were highly enriched and splenic cDC1 was obviously lower in percentage (**Figure 5C**). Cluster 7 (*Fabp5* and *S100a4* highly expressing cells) is exclusively comprised of cDC1 cells sourced from lymph nodes, with a striking absence of cDC1 cells from the spleen and aorta (**Figure 5C**). To better visualize the enrichment of aortic Xcr1$^+$ cDC1 cells distributed in a few clusters, we separately compared the three samples from the spleen, lymph nodes, and aorta of hyperlipidemic mice using density plots. Interestingly, the Xcr1$^+$ cDC1 cells from the spleen and lymph nodes displayed an obvious difference in their distribution, and aortic Xcr1$^+$ cDC1 cells appeared more enriched in a few clusters (**Figure 5D-E**). Therefore, our data suggest that Xcr1$^+$ cDC1 cells from the spleen and lymph nodes can differ markedly in heterogeneity, and aortic Xcr1$^+$ cDC1 cells are enriched in a few clusters that express marker genes, *Ccr2*, *Sept3*

264 and *Cldnd1* (**Supplementary Table 2**). Using the scRNA seq data of Xcr1^{+} cDC1 sorted from
265 hyperlipidemic mice, we annotated the 10 populations as shown in Figure S9A, following the
266 methodology from a previous study [41]. *Ccr7*$^{+}$ mature cDC1s (Cluster 3, 7 and 9) and *Ccr7-*
267 immature cDC1s (remaining clusters) were identified across cDC1 cells sorted from aorta, spleen
268 and lymph nodes (Figure S9B). Further stratification based on marker genes reveals that Cluster 10
269 is the pre-cDC1, with high expression level of *CD62L (Sell)* and low expression level of *CD8a*
270 (Figure S9C). Cluster 6 and 8 are the proliferating cDC1s, which express high level of cell cycling
271 genes *Stmn1* and *Top2a* (Figure S9D). Cluster 1 and 4 are early immature cDC1s, and cluster 2 and
272 5 are late immature cDC1s, according to the expression pattern of *Itgae*, *Nr4a2* (Figure S9E). Cluster
273 9 cells are early mature cDC1s, with elevated expression of *Cxcl9* and *Cxcl10* (Figure S9F). Cluster
274 3 and 7 as late mature cDC1s, characterized by the expression of *Cd63* and *Fscn1* (Figure S9G). As
275 shown in Figure 5C and Figure S9, the 10 populations displayed a major difference of aortic cDC1
276 cells that lack in pre-cDC1s (cluster 10) and mature cells (cluster 3, 7 and 9). Interestingly, in
277 hyperlipidemic mice splenic cDC1 possess only Cluster 3 as the late mature cells while the lymph
278 node cDC1 cells have two late mature populations namely Cluster 3 and Cluster 7. In further
279 analysis, we also compared splenic cDC1 cells from HFD mice to those from ND mice. As shown
280 in Figure S10, HFD appears to impact early immature cDC1-1 cells (Cluster 1) and increases the
281 abundance of late immature cDC1 cells (Cluster 2 and 5), regardless of the fact that all 10
282 populations are present in two origins of samples. We also found that *Tnfaip3* and *Serinc3* are among
283 the most upregulated genes, while *Apol7c* and *Tifab* are downregulated in splenic cDC1 cells sorted
284 from HFD mice.
285 Together, these data implied that Xcr1^{+} cDC1 in the aorta originate from bone marrow, and Xcr1^{+}

286 cDC1 cells exhibit strong heterogeneity among aorta, spleen and lymph nodes.

287 **Knockout of Xcl1 attenuates the development of atherosclerosis in ApoE$^{-/-}$ mice**

288 Xcl1 is the major chemokine involved in cDC1 recruitment [42, 43], and plays critical role in
289 immune response with diverse physical and pathological implication through its interaction with the
290 sole receptor, Xcr1 [44, 45]. We found the presence of Xcl1 in the lesion area in both human and
291 mouse atherosclerotic lesions (data not shown). To elucidate the causal relationship between Xcl1
292 and Xcr1^{+} cDC1 in the development of atherosclerosis, and more importantly to experimentally
293 verify Xcl1 as a potential therapeutic target for atherosclerosis treatment, we established the Xcl1
294 and ApoE double knockout mice. After being fed with a HFD for 19 weeks, both Xcl1$^{-/-}$ ApoE$^{-/-}$
295 and ApoE$^{-/-}$ mice were sacrificed to assess the severity of atherosclerosis. As shown in **Figure 6A-**
296 **D**, the size of lesion at the descending aorta and aortic root was significantly smaller in Xcl1$^{-/-}$
297 ApoE$^{-/-}$ compared to that in ApoE$^{-/-}$ mice. Importantly, ORO staining of the liver, body weight and
298 blood lipid profiles revealed no significant differences between the two groups (**Figure 6E-H**).
299 Moreover, the IHC experiment result show the percentage of CD68 positive macrophages in aortic
300 lesion was similar between two groups (**Figure 6I-J**).

301 Previous study identified that Xcl1 serves as a potent chemokine, selectively acting on cDC1 cells
302 through its exclusive receptor, Xcr1 [43]. Consequently, we examined the DCs and the activation of
303 T cells in different organs, including aorta, lymph node and spleen. The flow cytometric results
304 illustrated that both frequencies and absolute counts of Xcr1^{+} cDC1 cells in the aorta were
305 significantly reduced, but cDCs and cDC2 cells from Xcl1$^{-/-}$ ApoE$^{-/-}$ were comparable with that
306 from ApoE$^{-/-}$ (**Figure 7A-C**). Moreover, in both lymph node and spleen, the absolute numbers of
307 pDC, cDC1 and cDC2 from Xcl1$^{-/-}$ ApoE$^{-/-}$ were comparable with that from ApoE$^{-/-}$ (**Figure S11**).

308 Crucially, $CD69^+$ frequency and CD44 MFI remained comparable in both aortic $CD4^+$ and $CD8^+$ T
309 cells between two groups (**Figure 7D-F**). However, aortic $CD8^+$ T cells exhibited reduced frequency
310 and absolute count, while $CD4^+$ T cells showed increased frequency but unchanged counts in $Xcl1^{-}$
311 $^{/-}$ $ApoE^{-/-}$ mouse versus controls (**Figure 7G** and **H**). Furthermore, the absolute numbers of $CD4^+$,
312 $CD8^+$, $CD4^+$ $CD69^+$ and $CD8^+$ $CD69^+$ T cells in both lymph node and spleen from $Xcl1^{-/-}$ $ApoE^{-/-}$
313 mouse were comparable with that from $ApoE^{-/-}$ mouse (**Figure S12)**.
314 Collectively, these data suggest that Xcl1 promotes atherosclerosis by recruiting $Xcr1^+$ cDC1 cells,
315 and facilitating $CD8^+$ T cell accumulation in lesions. More importantly, *in vivo* data demonstrated
316 the promising potential of targeting Xcl1 to reduce the inflammatory response in atherosclerotic
317 lesions. Our work paves the way to discover novel solutions for the treatment of atherosclerosis by
318 targeting Xcl1 and $Xcr1^+$ cDC1 cells.

319 **Discussion**

320 Atherosclerosis is a complex disorder, and understanding the role of the immune system,
321 particularly dendritic cells (DCs), is of paramount importance [46, 47]. The marked diversity of DC
322 subsets and their distinct, and at times contradictory functions pose challenges in clarifying the role
323 of each specific type of DC in the context of atherosclerosis [48-54]. Moreover, the restricted
324 characterization of each subset of DCs in atherosclerosis, especially when compared to that in well-
325 studied organs such as the skin and lymph nodes [13], has been severely hindered by the limited
326 application of appropriate genetic models and *in vivo* data. Equally significant is that dissecting the
327 functions of each subset of DCs *in vivo* relies on the development of genetic tools validated for
328 lineage specificity. Recently, $Xcr1^+$ cDC1 has been extensively investigated using the Cre line under
329 the promoter of the Xcr1, despite well-documented expression leakiness [20, 31]. Compelling

330 evidence from tumor and viral infection models [14, 42, 55-57], as well as metabolic disorders like
331 non-alcoholic steatohepatitis [58], has demonstrated the critical role of Xcr1^{+} cDC1 cells in diseases.
332 Nevertheless, the precise role of Xcr1^{+} cDC1 cells in atherosclerosis remains undetermined.
333 The precise characterization of Xcr1^{+} cDC1 and its functions within the atherosclerotic milieu could
334 provide valuable insights into the immunopathogenesis of the disease. By delineating the specific
335 contributions of Xcr1^{+} cDC1, we may identify novel therapeutic targets and develop more targeted
336 and effective strategies for the prevention and treatment of atherosclerosis. Therefore, investigation
337 to understand the roles of Xcr1^{+} cDC1 in the context of atherosclerosis and to identify therapeutic
338 targets is highly warranted. However, at least two major obstacles impede the *in vivo* study of Xcr1^{+}
339 cDC1 in atherosclerotic mice. First, Xcr1^{+} cDC1 cells are extremely scarce in number, and it is quite
340 challenging to obtain highly purified Xcr1^{+} cDC1 cells from aortic plaque in hyperlipidemic mice.
341 Second, there are very few appropriate genetic model systems that permit functional analyses of
342 Xcr1^{+} cDC1 *in vivo*. Earlier studies on the role of Xcr1^{+} cDC1 cells in atherosclerosis have yielded
343 conflicting results, largely due to the use of different mouse models. For instance, the deletion of
344 Batf3, Irf8, Dngr1, or Flt3 decreased the cDC1 cells. Nevertheless, Batf3 deficiency had no impact
345 on atherosclerosis in hyperlipidemic mice. In contrast, Irf8 or Dngr1 deficiency reduced the
346 development of atherosclerosis, while Flt3 deficiency exacerbated the condition [15-19]. The
347 recently developed Xcr1-Cre was found to have leakiness of recombinase activity in other immune
348 cells [20]. Here, we optimized the design for the construction of the Cre line using the endogenous
349 promoter of Xcr1 and validated its fidelity under hyperlipidemic conditions. We crossed the novel
350 knock-in line termed Xcr1$^{Cre\text{-}Gfp}$ with Rosa26$^{LSL\text{-}tdRFP}$ Cre reporter mice and used the resulting F1
351 hybrids as bone marrow donors. The bone marrow cells were then transferred into ApoE$^{-/-}$ mice,

352 which were subsequently fed on a HFD. We monitored the Cre recombinase activity, which was
353 reflected by the tdRFP expression of this novel mouse line. Under hyperlipidemic conditions, we
354 did not observe any leakiness of Cre activity, as tdRFP was strictly restricted to cDC1 cells. To the
355 best of our knowledge, this novel Cre line is the first of its kind. We further crossed the $Xcr1^{Cre\text{-}Gfp}$
356 and $Rosa26^{LSL\text{-}DTA}$ mice with $ApoE^{-/-}$ mice respectively. Subsequently, by further crossing, we
357 obtained $Xcr1^{Cre\text{-}Gfp}$ $Rosa26^{LSL\text{-}DTA}$ $ApoE^{-/-}$ mice to create a complex genetic model, in which $Xcr1^{+}$
358 cDC1 is depleted *in vivo* in the context of atherosclerosis. Very interestingly, in the $Xcr1^{+}$ cDC1
359 depleted mice, atherosclerosis was significantly ameliorated. Coupled with the data we obtained
360 from murine and human samples, where $Xcr1^{+}$ cDC1 cells exist in the aortic plaque and their
361 accumulation is correlated with disease progression, we conclude that $Xcr1^{+}$ cDC1 is essential for
362 the development of atherosclerosis.
363 Despite the fact that $Xcr1^{+}$ cDC1 cells are extremely rare in number, we were inclined to understand
364 if there were any differences among $Xcr1^{+}$ cDC1 cells from different organs. Firstly, we determined
365 that the $Xcr1^{+}$ cDC1 in the aortic plaque is replenished by circulating precursors using the bone
366 marrow transfer model. Then we compared, under hyperlipidemic conditions, the $Xcr1^{+}$ cDC1 cells
367 sorted from the spleen and lymph nodes, supplemented by a small number of but well-purified $Xcr1^{+}$
368 cDC1 cells from aortic lesions. To our surprise, the clusters of $Xcr1^{+}$ cDC1 displayed obvious
369 distinctions among different organs. When the $Xcr1^{+}$ cDC1 cells from aortic lesions were projected
370 to the clusters, we found that the major subsets present in the lymph nodes, characterized by the
371 expression of markers *Ccl5 and Fabp5*, and in the spleen, marked by *Stk17b* and *Gpr171*, were
372 basically absent in the aorta. Meanwhile, compared with spleen and lymph nodes, the aortic $Xcr1^{+}$
373 cDC1 cells are highly expressed *Ccr2*, which is an extremely important chemokine receptor

374 dominating monocyte homing [59-61].

375 This pronounced tissue-specific compartmentalization of Xcr1^{+} cDC1 subsets may related to
376 multiple mechanisms including developmental imprinting that instructs precursor differentiation
377 into transcriptionally distinct subpopulations [62], and microenvironmental filtering through organ-
378 specific chemokine axes (e.g., CCL2/CCR2 in spleen) selectively recruits receptor-matched subsets
379 [63, 64]. This spatial specialization optimizes pathogen surveillance for local immunological
380 challenges. Based on the maturation analysis of the cDC1 scRNA seq data [41], our findings suggest
381 that the aortic cDC1 cells display a major difference from those of spleen and lymph nodes by
382 lacking the mature clusters, whereas lymph node cDC1 cells contain an additional *Fabp5*$^{+}$ *S100a4*$^{+}$
383 late mature Cluster. Our results also suggest that hyperlipidemia contributes to alteration in early
384 immature cDC1 and in the abundance of late immature cDC1 cells, which was associated with
385 dramatic change in gene expression of *Tnfaip3*, *Serinc3*, *Apol7c* and *Tifab*.

386 In other disease models, Xcr1^{+} cDC1 cells are crucial for activating T cells [56, 65], and we
387 confirmed that in hyperlipidemic mice, the depletion of cDC1 substantially attenuated T cell
388 activation responses. It is important to note that Xcr1^{+} cDC1 cells are known for well-established
389 role in cross-presentation to CD8^{+} T cells, recent studies have shown Xcr1^{+} cDC1 cells also engage
390 with CD4^{+} T cells [20, 27]. Our data showing Xcr1^{+} cDC1-dependent CD4 and CD8 T cell
391 activation in atherosclerotic plaques is in line with the new paradigm for cDC1s as a platform for
392 both CD4 and CD8 T cell responses in the novel context of atherosclerosis. Considering the
393 multifaceted roles of macrophages in lipid metabolism, inflammation, and plaque dynamics during
394 the development of atherosclerosis [66], we evaluated the presence of macrophages in
395 atherosclerotic lesions using IHC and flow cytometry. Our results indicated comparable proportions

of macrophages in the aorta between Xcr1^{+} cDC1 depleted mice and ApoE$^{-/-}$ control mice. Additionally, our results also demonstrated that the loss of Xcr1^{+} cDC1 cells did not affect lipid status.

Since we elucidated the critical role of Xcr1^{+} cDC1 cells in atherosclerosis, our aim was to test the therapeutic potential of inhibiting this specific cell type during disease progression. As Xcr1 is the sole receptor for Xcl1, and Xcl1 selectively attracts Xcr1^{+} cDC1 cells in both mice and humans [45, 67], we performed Xcl1 knockout on the background of ApoE deficient mice and assessed the impact on atherosclerosis development. We found that the Xcl1-Xcr1 axis plays a crucial role in the progression of atherosclerosis. Our results demonstrated that the loss of Xcl1 in hyperlipidemic ApoE$^{-/-}$ mice significantly reduced atherosclerotic lesion formation, decreased the frequencies and absolute coutns of Xcr1^{+} cDC1 cells and CD8^{+} T cells in the aorta, without affecting lipid status or the number of aortic macrophages. Notably, while complete ablation of Xcr1^{+} cDC1s impaired T cell activation, reduction of Xcr1^{+} cDC1 recruitment via Xcl1 deletion did not significantly compromise this process. This discrepancy may arise through compensatory mechanisms: alternative chemokine axes (e.g., CCL5/CCR5, CXCL9/CXCR3, BCL9/BCL9L) may partially rescue Xcr1^{+} cDC1 homing [13, 68, 69], while non-cDC1 antigen-presenting cells (e.g., monocytes, cDC2s) may sustain T cell activation [55, 70]. Furthermore, tissue-specific microenvironment factors could potentially modulate its role in other diseases. In summary, our findings identify Xcl1 as a potential therapeutic target for atherosclerosis therapy, though its cellular origins and regulation of lesional Xcr1^{+} cDC1 and T cells dynamics require further studies.

416 ## Materials and Methods

417 ### Animal experiments and patients

418 All mice were raised in a Specific Pathogen-Free facility and the experiments were conducted in
419 accordance with the guidelines approved by the Animal Ethics Committee of Xinxiang Medical
420 University (China) (Reference No. XYLL-2016S001). The sections of the human femoral artery
421 were obtained in accordance with our previous study [30] and approved by the Ethics Committee
422 of the Third Military Medical University (Project identification code SYXK-PLA-20170005).
423 Rosa26$^{LSL\text{-}RFP}$ knock-in mice were generously provided by Hervé Luche at University Clinics Ulm
424 in Germany [32]. C57BL/6 and ApoE$^{-/-}$ mice were purchased from Beijing Vital River Laboratory
425 Animal Technology (China). Rosa26$^{LSL\text{-}DTA}$ knock-in mice (Stock Number 009669) were purchased
426 from the Jackson Laboratory (United States of America). Both HFD (contained 20% protein, 20%
427 carbohydrate, 40% fat and 1.25% cholesterol, Cat: XT108C), and ND (contained 20% protein, 64%
428 carbohydrate, 20% fat, Cat: AIN-93G) were purchased from Jiangsu Xietong Pharmaceutical
429 Bioengineering Co., Ltd. 7-8 weeks old mice were used to establish atherosclerosis model through
430 fed on a HFD for 8-20 weeks. On harvest, each sample was assigned an analytical code that was
431 irrelevant to its genotype and processed and analyzed by a researcher blinded to its origin.

432 ### Generation of Xcr1$^{Cre\text{-}Gfp}$ knock-in mice

433 The Xcr1$^{Cre\text{-}Gfp}$ mouse line was generated by inserting a Cre-P2A-GFP-P2A cassette immediately
434 upstream of the endogenous *Xcr1* translational start codon (ATG). This design enables co-
435 expression of Cre recombinase and GFP under the control of the native *Xcr1* promoter. A 3.2-kb
436 repair template was synthesized (GenScript, Nanjing, China), consisting of a 0.62-kb 5' homology

437 arm (HA), a codon-optimized *Cre* sequence fused to a P2A peptide, an enhanced GFP reporter
438 linked to a second P2A site, and a 0.67-kb 3' homology arm. For targeted integration, CRISPR/Cas9-
439 mediated homology-directed repair (HDR) was performed by co-injecting Cas9 mRNA, a chimeric
440 sgRNA (sgXcr1-KI), and the repair template into fertilized C57BL/6 zygotes at the one-cell stage,
441 following established protocols[71, 72]. Founders (F0) harboring the correct knock-in allele were
442 identified by PCR and Sanger sequencing, then used to establish heterozygous lines. The sgRNA
443 sequence is provided in **Supplementary Table 3**.

444 **Breeding strategy of Xcr1$^{Cre\text{-}Gfp}$ Rosa26$^{LSL\text{-}DTA}$ ApoE$^{-/-}$**

445 To generate Xcr1$^{Cre\text{-}Gfp}$ Rosa26$^{LSL\text{-}DTA}$ ApoE$^{-/-}$ mice, we performed the following crosses: Xcr1$^{Cre\text{-}}$
446 ^{Gfp} mice were crossed with ApoE$^{-/-}$ mice, and offspring heterozygous for both alleles were
447 intercrossed to obtain homozygous Xcr1$^{Cre\text{-}Gfp}$ ApoE$^{-/-}$ mice. Rosa26$^{LSL\text{-}DTA}$ mice were crossed with
448 ApoE$^{-/-}$ mice, and progeny heterozygous for both alleles were intercrossed to generate homozygous
449 Rosa26$^{LSL\text{-}DTA}$ ApoE$^{-/-}$ mice. Finally, homozygous Xcr1$^{Cre\text{-}Gfp}$ ApoE$^{-/-}$ mice were crossed with
450 homozygous Rosa26$^{LSL\text{-}DTA}$ ApoE$^{-/-}$ mice to produce Xcr1$^{Cre\text{-}Gfp}$ Rosa26$^{LSL\text{-}DTA}$ ApoE$^{-/-}$ offspring.

451 **Generation of Xcl1 knockout mice**

452 The Xcl1 knockout mouse line was generated using CRISPR/Cas9 genome editing through the
453 microinjection of a mixture containing Cas9 mRNA and two sgRNAs into fertilized C57BL/6
454 zygotes at the one-cell stage, as previously described [73]. The genotypes were confirmed using
455 PCR and Sanger sequencing. Subsequently, Xcl1 and ApoE double knockout mice were obtained
456 by crossing the Xcl1$^{-/-}$ mice with ApoE$^{-/-}$ mice. The sequences of the sgRNA are reported in
457 **Supplementary Table 3**.

458 **Bone marrow transplantation**

459 After one week of antibiotic treatment, the recipient CD45.1^{+} CD45.2^{+} ApoE$^{-/-}$ mice were injected
460 intraperitoneally with busulfan at a dosage of 30 μg/g every two days for one week. Subsequently,
461 bone marrow from 8-week-old CD45.2^{+} Xcr1$^{Cre\text{-}Gfp}$ Rosa26$^{LSL\text{-}RFP}$, CD45.2^{+} Xcr1$^{Cre\text{-}Gfp}$ Rosa26$^{LSL\text{-}}$
462 ^{DTA} or WT (CD45.2^{+} wild-type) donor mice was intravenously transferred to each recipient mouse,
463 with two million cells administered per recipient. The efficiency of transplantation was assessed
464 four-week post-transplantation, after which all mice were fed a HFD for 16 weeks. Finally, the mice
465 were sacrificed for *en face* analysis of the descending aorta, hematoxylin and eosin (H&E) staining,
466 Oil Red O (ORO) staining of the aortic root, and flow cytometry analysis, as previously described
467 [74].

468 **Immunofluorescence**

469 Frozen sections of the aortic root from mice were incubated at 60 °C for 2 minutes and then fixed
470 in 4% paraformaldehyde for 30 minutes. The samples were subsequently washed with PBS and
471 permeabilized/blocked with 0.1% Triton X-100 in 5% BSA. Next, the primary antibodies, including
472 anti-Xcr1 (BD Biosciences, Cat. 148212) and anti-CD11c (BD Biosciences, Cat. 12-0114-83), were
473 applied in a wet box at 4 °C overnight. After washing with PBST (PBS containing 0.1% Tween-20)
474 for five times, the samples were incubated with secondary antibodies for 1 hour, followed by a 10-
475 minute incubation with DAPI at room temperature (protected from light). The fluorescent signals
476 of the sections were detected using a Nikon C2 confocal microscope (Nikon, Japan).

477 **Morphometric and immunohistochemical analyses**

478 After modeling, the heart and aorta tissue were obtained from mice. The *en face* descending aortas

479 were fixed with 4% paraformaldehyde and subsequently stained with ORO. Additionally, frozen
480 sections of the aortic roots were stained with ORO and H&E to assess the severity of atherosclerosis,
481 and frozen sections of livers were stained with ORO to assess the severity of lipid accumulation, in
482 accordance with our previous study [74]. Paraffin-embedded sections of the aortic root were
483 dewaxed in xylene twice for 10 minutes, rehydrated through descending grades of ethanol, and
484 subjected to sodium citrate-induced antigen retrieval for 10 minutes at 95 °C. The sections were
485 then incubated with 3% H_2O_2 for 10 minutes at room temperature. Following this, the sections were
486 blocked and incubated with primary antibodies, either anti-Xcr1 (NBP1-02343) or CD68
487 (FB113109). After five washes with DPBS, the sections were incubated with secondary antibodies
488 for 30 minutes and stained with DAB at room temperature. Subsequently, the sections were
489 counterstained with hematoxylin, dehydrated in ethanol, and mounted with neutral balsam. Images
490 were captured using the digital pathology system (Pannoramic MIDI, Hungary), viewed using
491 CaseViewer2.4 software and analyzed using ImageJ software.

492 **Flow cytometry analysis**

493 To obtain the single-cell suspension, aortas, lymph nodes and spleens were collected from each
494 mouse. Spleens were directly dissociated using the Gentle MACS Dissociators (Miltenyi Biotec).
495 Aortas and lymph nodes were cut into small pieces and then dissociated using the Gentle MACS
496 Dissociators. Dissociated tissues digested with digestive enzymes (Collagenase IV, Cat: V900893
497 from Sigma; DNase I, Cat: DN25 from Sigma; Liberase DH, Cat: 5401054001 from Roche) for 30
498 minutes at 37 °C using a shaker set to 300 rpm or a heating block. The resulting cell suspension was
499 filtered through 75 μm strainers and subsequently blocked with 2.4G2 for 20 minutes at 4 °C,
500 followed by washing with stain buffer (BD, Cat: 554656). Then samples were stained with

501 monoclonal antibody mixes for 30 minutes at 4 °C followed by washing with stain buffer. Finally,
502 cells were resuspended in stain buffer containing 200 nM Sytox blue (ThermoFisher Scientific, Cat:
503 S34857) and acquired using a flow cytometer (ThermoFisher Scientific, Invitrogen Attune NxT
504 Flow Cytometer), and the FACS data were analyzed using FlowJo software. The following
505 antibodies purchased from BioLegend, BD or eBioscience were used to detect surface markers by
506 flow cytometry: anti-CD45.2 (104) conjugated to eFluor 450, FITC or PE-Cy7; anti-CD45.1 (A20)
507 conjugated to PE or eFluor450; anti-CD45 (30-F11) conjugated to PE; anti-CD11b (M1/70)
508 conjugated to super Bright 600, BUV395 or biotin; anti-CD3e (145-2C11) conjugated to PE-Cy5.5
509 or PE-Cy7; anti-CD3e (eBio500A2) conjugated to Alexa Fluor700; anti-CD19 (eBio1D3)
510 conjugated to PE-Cy5.5 or biotin; anti-Xcr1 (ZET) conjugated to APC or BV650; anti-Ly6G (1A8)
511 conjugated to Alexa Fluor 700; anti-MHCII (M5/114.15.2) conjugated to APC-eFluor780; anti-
512 CD11c (N418) conjugated to PE or PE-Cy5.5; anti-Siglec H (eBio440c) conjugated to PE-Cy7 or
513 PE; anti-CD8b (eBioH35-17.2) conjugated to eFluor 450; anti-CD44 (IM7) conjugated to BV605;
514 anti-CD4 (RM4-5) conjugated to PE-Cy5.5; anti-CD69 (H1.2F3) conjugated to PE-Cy7; anti-
515 CD62L (MEL-14) conjugated to APC; anti-CD5 (53-7.3) conjugated to APC-eFluor780 or biotin;
516 anti-Siglec F (E50-2440) conjugated to BV421; anti-F4/80 (BM8) conjugated to PE-Cy7; anti-
517 CD64 (X54-5/7.1) conjugated to APC; anti-NK1.1 (PK136) conjugated to Alexa Fluor 700; anti-
518 CD172α (P84) conjugated to FITC.

519 **Single cell RNA sequencing**

520 Eight-week-old male ApoE$^{-/-}$ mice were fed with 20-week ND or HFD. The single cell suspension
521 of spleen, lymph node and aorta were obtained according to the flow cytometry analysis section.
522 Single cell suspension from spleens and lymph nodes were firstly removed the CD5^{+}, CD19^{+} and

523 CD11b^{+} cells via SAV conjugated beads. Then two million live cells from spleen and lymph node
524 were stained with mix1 (CD45.2-PE-Cy7, CD11c-PE-Cy5.5, CD172α-FITC, MHCII- APC-
525 eFluor780 and Xcr1-APC), and all cells from aorta were stained with mix2 (CD45.2-PE-Cy7,
526 CD11b-super bright 600, CD11c-PE-Cy5.5, MHCII- FITC, CD3- Alexa Fluor 700, CD19- Alexa
527 Fluor 700, Ly6G- Alexa Fluor 700 and Xcr1-APC) for 30 minutes at 4 °C. After washing with 1 mL
528 FACS buffer two times, cells from different organs were stained with different anti-CD45 antibodies
529 conjugated with barcode oligos from BD™ Ms Single Cell Sample Multiplexing Kit (BD
530 Bioscience, Cat: 633793). Finally, cells were resuspended with Sytox blue and CD11c^{+} MHCII^{+}
531 Xcr1^{+} cells were sorted and subjected to the BD Rhapsody Express system. Then cDNA and sample
532 tag libraries were built with BD Rhapsody whole transcriptome amplification (WTA) reagent kit
533 (BD Bioscience, Cat: 633733, 633773, 633801, 664887) following manufacturer's instructions, and
534 sequenced on an illumine Novaseq 600 sequencer. Pair-end Fastq files of sample tag and WTA data
535 were processed via BD Rhapsody^{TM} analysis pipeline v2.0, and the resultant dataset was mainly
536 analysis using SeqGeq^{TM} software, which contain Lex-BDSMK and Seurat v4.04 plugin
537 components. Raw data and processed data were uploaded into GEO (Accession number:
538 GSE279370).

539 **Statistical analysis**

540 All data were presented as means ± SEM (Standard Error of the Mean), reflecting the average values
541 of biological measurements across multiple samples. Data analysis was performed using GraphPad
542 Prism software (version 8.0). Statistical significance was assessed by both parametric (unpaired
543 Student's *t*-test) and nonparametric (Mann–Whitney test) methods when comparing two groups.
544 The assumptions of the tests were checked to ensure appropriate application. Significant differences

between different groups were set at * $P<0.05$, ** $P<0.01$, *** $P<0.001$ and **** $P<0.0001$. Graphical representations of the data will include bar graphs with error bars denoting SEM.

Acknowledgements

We thank the animal facility and flow cytometry facility of GRIS in Xinxiang Medical University for providing technical support and assistance. Generation of murine genetic models were supported by 111 program (D20036).

Author Contributions

Lichen Zhang and **Yinming Liang** conceived the project. **Tianhan Li** and **Liaoxun Lu** wrote the manuscript and carried out the majority of the experiments. **Bernard Malissen** and **Lichen Zhang** designed the Xcr1Cre-Gfp knock-in mice and Xcl1 knockout mice. **Juanjuan Qiu**, **Xin Dong**, **Le Yang**, **Kexin He**, and **Yanrong Gu** assisted in the experimental procedures. **Binhui Zhou** performed cell sorting for scRNA sequencing. **Tingting Jia** and **Rong Huang** contributed to data curation and validation. **Toby Lawrence**, **Marie Malissen**, and **Hui Wang** participated in the manuscript review and editing. **Guixue Wang** assisted in the preparation of human samples. **Yinming Liang**, **Lichen Zhang**, and **Tianhan Li** contributed to obtaining the funding for the project.

Sources of Funding

This research was funded by grants from Science and Technology Innovation Program of Hunan Province [2023DK2005], [2024RC1071] and [2022RC1223], and NSFC grants 32170879 and 82301972, and Science and Technology Department of Henan Province 242102310030.

Declaration of competing interest

The authors declare no competing interests.

568 ## Figure legends

569 **Figure 1. Progressive accumulation of Xcr1^{+} cDC1 cells in human and mouse advanced**
570 **atherosclerotic lesions**

571 **A**, Representative images of immunohistochemical staining demonstrate Xcr1 expression in normal
572 areas and plaque areas of the femoral artery from three cardiovascular disease patients. **B**,
573 Quantitative analysis of the Xcr1-positive area in normal area and plaque regions. **C**, Representative
574 immunofluorescence images depict DAPI (blue), Xcr1 (green) and CD11c (red) within the lesions
575 of aortic root of ApoE$^{-/-}$ mice fed with 16-week ND or HFD. **D**, Quantitative analysis of Xcr1 and
576 CD11c double positive area in lesion area (n = 6). Scale bars, 100 μm. **E**, Representative images
577 depicting immunohistochemical staining of Xcr1 in lesions of the aortic root of ApoE$^{-/-}$ mice fed a
578 HFD for varying durations. **F**, Quantitative analysis of the Xcr1-positive area in the lesion regions.
579 (8-week HFD, n = 11; 12-week HFD, n = 15; 16-week HFD, n = 29). Data represent as mean ±
580 SEM. * $P<0.05$. *** $P<0.001$.**** $P<0.0001$.

581

582 **Figure 2. Selective expression of Xcr1$^{Cre\text{-}Gfp}$ in cDC1 cells.**

583 **A**, Diagram illustrating the bone marrow transfer process. **B** and **C**, Representative flow cytometric
584 analysis and corresponding quantification of GFP^{+}RFP^{+} in cDC1 and non-cDC1 populations within
585 the cDC1 and non-cDC1 populations of the spleen. These data were obtained from ApoE$^{-/-}$ mice
586 that had received bone marrow transplants from either WT or Xcr1$^{Cre\text{-}Gfp}$ Rosa26$^{LSL\text{-}RFP}$ donors and
587 were maintained on a HFD for 16 weeks (WT, n = 4; Xcr1$^{Cre\text{-}Gfp}$ Rosa26$^{LSL\text{-}RFP}$, n = 3). **D** and **E**,
588 Representative flow cytometric analysis and quantification of the percentage of GFP^{+} cells among
589 pDC, cDC1 and cDC2 cells populations in the spleen. **F**, Quantification of the percentage of pDC,

590 cDC1 and cDC2 cells in spleen. (D-F, ApoE$^{-/-}$, Xcr1$^{Cre\text{-}Gfp}$ ApoE$^{-/-}$ and Xcr1$^{Cre\text{-}Gfp}$ Rosa26$^{LSL\text{-}DTA}$

591 ApoE$^{-/-}$ mice fed with a HFD for 16 weeks, n = 3). Data represent as mean ± SEM. **** P<0.0001;

592 NS, non-significant.

593

594 **Figure 3. Specific depletion of Xcr1^{+} cDC1 cells in ApoE$^{-/-}$ mice reduces atherosclerosis**

595 **progression with no effect on macrophages.**

596 **A**, ORO staining of the descending aortas. Scale bar, 5 mm. **B**, Quantification of the lesion area in

597 the descending aorta (ApoE$^{-/-}$ mice, n = 9; Xcr1$^{Cre\text{-}Gfp}$ Rosa26$^{LSL\text{-}DTA}$ ApoE$^{-/-}$ mice, n = 6). **C**, ORO

598 and H&E staining of the aortic roots of representative mice from each group. **D**, Quantification of

599 lesion area in the aortic root. (ApoE$^{-/-}$ mice, n = 7; Xcr1$^{Cre\text{-}Gfp}$ Rosa26$^{LSL\text{-}DTA}$ ApoE$^{-/-}$ mice, n = 8).

600 Scale bar, 200 μm. **E** and **F**, H&E staining and quantification of necrotic core area in the lesions of

601 aortic root. (ApoE$^{-/-}$ mice, n = 7; Xcr1$^{Cre\text{-}Gfp}$ Rosa26$^{LSL\text{-}DTA}$ ApoE$^{-/-}$ mice, n = 8). Scale bar, 200 μm.

602 **G** and **H**, Representative flow cytometric analysis and quantification of macrophages in the aorta.

603 (ApoE$^{-/-}$ mice, n = 8; Xcr1$^{Cre\text{-}Gfp}$ Rosa26$^{LSL\text{-}DTA}$ ApoE$^{-/-}$ mice, n = 6). **I** and **J,** Representative

604 immunohistochemical staining images of CD68 and quantification of CD68 positive area in the

605 lesions of the aortic root. (ApoE$^{-/-}$ mice, n = 6; Xcr1$^{Cre\text{-}Gfp}$ Rosa26$^{LSL\text{-}DTA}$ ApoE$^{-/-}$ mice, n = 8). Scale

606 bar, 100 μm. ApoE$^{-/-}$ and Xcr1$^{Cre\text{-}Gfp}$ Rosa26$^{LSL\text{-}DTA}$ ApoE$^{-/-}$ mice were fed on a 16-week HFD to

607 develop atherosclerosis. Data represent as mean ± SEM. NS, non-significant. ** P<0.01. ***

608 P<0.001.

609

610 **Figure 4. Specific depletion of Xcr1^{+} cDC1 cells in ApoE$^{-/-}$ mice decreases T cell activation**

611 **within aorta.**

612 **A**, Representative flow cytometric analysis cDC1 cells in aortas. **B** and **C**, Quantification of the
613 frequencies and absolute counts of cDC1 cells in aorta (n = 4). **D**, Representative flow cytometric
614 analysis T cells in aortas. **E** and **F**, Quantification of the frequencies and absolute counts of total T,
615 $CD4^+$ and $CD8^+$ T cells in aortas. **G**, Quantification of the frequencies of $CD4^+CD69^+$ and $CD8^+$
616 $CD69^+$ in aortas. **H**, Quantification of the MFI of CD44 in $CD4^+$ and $CD8^+$ T cells in aortas. **(**D-G,
617 $ApoE^{-/-}$ mice, n = 8, $Xcr1^{Cre\text{-}Gfp}$ $Rosa26^{LSL\text{-}DTA}$ $ApoE^{-/-}$ mice, n = 7, fed on a HFD for 16 weeks).
618 Data represent as mean ± SEM. * $P<0.05$, ** $P<0.01$, *** $P<0.001$, NS, non-significant.
619

620 **Figure 5. Sc-RNA sequencing analysis of the aorta, lymph nodes and spleen in $ApoE^{-/-}$ mice**
621 **fed with a 20-week HFD.**

622 **A**, UMAP plot delineates 10 annotated cell types of $Xcr1^+$ cDC1 cells from aorta, lymph node and
623 spleen in $ApoE^{-/-}$ mice maintained on a HFD or ND for 20 weeks. **B**, Heatmap statistic map displays
624 the top ten up-regulated genes across various clusters. **C**, The proportion of 10 clusters among
625 groups. **D** and **E**, UMAP plot representing $Xcr1^+$ cDC1 cells from aorta, lymph nodes, spleen, and
626 a merged plot in $ApoE^{-/-}$ mice maintained on a HFD for 20 weeks.
627

628 **Figure 6. Xcl1 deficiency reduces atherosclerotic lesion formation in $ApoE^{-/-}$ mice.**

629 **A**, ORO staining of the descending aortas. Scale bar, 5 mm. **B**, Quantification of the lesion area in
630 aortas. **C**, ORO and H&E staining of aortic roots. Scale bar, 200 μm. **D**, Quantification of the lesion
631 area in aortic roots. **E** and **F**, Representative liver images and quantification of ORO positive area
632 in livers (n = 24 regions from 8 mice, 3 regions per mice). Scale bar, 100 μm. **G**, The concentrations
633 of TC, TG, LDL and HDL in the serum. **H**, Body weight of mice before and after feeding with 19-

634 week HFD. **I**, Representative immunohistochemical staining of CD68 in aortic roots. **J**,
635 Quantification of CD68 positive area in the lesions of aortic roots (n = 24 lesions from 8 mice, 3
636 lesions per mice). Scale bar, 100 μm. ApoE$^{-/-}$ mice and Xcl1$^{-/-}$ ApoE$^{-/-}$ mice fed a HFD for 19
637 weeks (n = 8 per group). Data represent as mean ± SEM. ** P<0.01, *** P<0.001, NS, non-
638 significant.

639

640 **Figure 7. Xcl1 deficiency reduces CD8^{+} T cells in the aortas from ApoE$^{-/-}$ mice.**

641 **A**, Representative flow cytometric analysis of cDC, cDC1 and cDC2 cells in aortas. **B** and **C**,
642 Quantification of the frequencies and absolute counts of cDC, cDC1 and cDC2 cells in aortas (n =
643 7). **D**, Representative flow cytometric analysis of T cell subsets in aortas, including CD3e^{+} CD5^{+},
644 CD4^{+}, CD4^{+} CD69^{+}, CD8^{+} and CD8^{+} CD69^{+} T cells. **E**, Quantification of the frequencies of
645 CD4^{+}CD69^{+} and CD8^{+} CD69^{+} in aortas. **F**, Quantification of the MFI of CD44 in CD4^{+} and CD8^{+}
646 T cells in aortas. **G** and **H**, Quantification of the frequencies and absolute counts of CD3e^{+} CD5^{+},
647 CD4^{+} and CD8^{+} cells in aortas. (D-H, ApoE$^{-/-}$ mice (n = 5) and Xcl1$^{-/-}$ApoE$^{-/-}$ mice (n = 6) fed
648 with a 16-week HFD). Data represent as mean ± SEM. * P<0.05, NS, non-significant.

649

650 **Figure S1. Schematic diagram illustrating the knock-in of the 5'HA-iCre-P2A-EGFP-P2A-**
651 **3'HA vector into the mouse Xcr1 locus**.

652

653 **Figure S2. Flow cytometric analysis of cDC1 cells in the lymph nodes and spleens of ApoE$^{-/-}$**
654 **mice and Xcr1$^{Cre\text{-}Gfp}$ Rosa26$^{LSL\text{-}DTA}$ ApoE$^{-/-}$ mice fed a 7-weeks ND.**

655 **A**, Representative flow cytometric analysis of cDC1 cells in lymph nodes. **B**, Quantification of the

656 frequencies and number of cDC1 cell in lymph nodes. **C**, Representative flow cytometric analysis
657 cDC1 cells in the spleens. **D**, Quantification of the frequencies and number of cDC1 cell in the
658 spleens. ApoE$^{-/-}$ mice and Xcr1$^{Cre\text{-}Gfp}$ Rosa26$^{LSL\text{-}DTA}$ ApoE$^{-/-}$ mice fed with 7-week ND, n = 7. Data
659 represent the mean ± SEM. *** P<0.001.

660

661 **Figure S3. Lipid profile, body weight and ORO staining of the liver in ApoE$^{-/-}$ mice and**
662 **Xcr1$^{Cre\text{-}Gfp}$ Rosa26$^{LSL\text{-}DTA}$ ApoE$^{-/-}$ mice fed a 16-week HFD.**

663 **A**, Concentrations of TC, TG, LDL and HDL in the serum. **B**, Body weight measurements of both
664 groups of mice. **C**, ORO staining of liver from each group. Scale bar, 100 μm. **D**, Quantification of
665 ORO positive area in liver. ApoE$^{-/-}$ mice (n =7) and Xcr1$^{Cre\text{-}Gfp}$ Rosa26$^{LSL\text{-}DTA}$ ApoE$^{-/-}$ mice (n =8)
666 were fed on a 16-week HFD to develop atherosclerosis. Data represent the mean ± SEM. NS, non-
667 significant.

668

669 **Figure S4. Flow cytometric analysis of cDC1 cells in the lymph nodes and spleens of ApoE$^{-/-}$**
670 **and Xcr1$^{Cre\text{-}Gfp}$ Rosa26$^{LSL\text{-}DTA}$ ApoE$^{-/-}$ mice fed a 16-week HFD.**

671 **A**, Representative flow cytometric analysis of cDC1 cells in lymph nodes. **B**, Quantification of the
672 frequencies and numbers of cDC1 cells in lymph nodes. **C**, Representative flow cytometric analysis
673 of cDC1 cells in the spleens. **D**, Quantification of the frequencies and numbers of cDC1 cells in the
674 spleens. ApoE$^{-/-}$ mice (n =7) and Xcr1$^{Cre\text{-}Gfp}$ Rosa26$^{LSL\text{-}DTA}$ ApoE$^{-/-}$ mice (n =8) were fed on a 16-
675 week HFD. Data represent the mean ± SEM. *** P<0.001.

676

677 **Figure S5. Flow cytometric analysis of T cells in the lymph nodes and spleens of ApoE$^{-/-}$ mice**

and Xcr1$^{Cre\text{-}Gfp}$ Rosa26$^{LSL\text{-}DTA}$ ApoE$^{-/-}$ mice fed a 16-week HFD.

A, Representative flow cytometric analysis of CD4$^+$, CD8$^+$, CD4$^+$CD69$^+$ and CD8$^+$CD69$^+$ T cells in lymph nodes. **B** and **C**, Quantification of the frequencies and numbers of CD4$^+$, CD8$^+$, CD4$^+$ CD69$^+$ and CD8$^+$ CD69$^+$ T cells in lymph nodes. **D**, Representative flow cytometric analysis and quantification of CD4$^+$, CD8$^+$, CD4$^+$ CD69$^+$ and CD8$^+$ CD69$^+$ T cells in the spleens. **E** and **F**, Quantification of the frequencies and numbers of CD4$^+$, CD8$^+$, CD4$^+$ CD69$^+$ and CD8$^+$CD69$^+$ T cells in the spleens. ApoE$^{-/-}$ mice (n =7) and Xcr1$^{Cre\text{-}Gfp}$ Rosa26$^{LSL\text{-}DTA}$ ApoE$^{-/-}$ mice (n =8) were fed on a 16-week HFD. Data represent the mean ± SEM. * P<0.05, ** P<0.01, *** P<0.001, NS, non-significant.

Figure S6. T cells analysis in the lymph nodes and spleens of ApoE$^{-/-}$ mice and Xcr1$^{Cre\text{-}Gfp}$ Rosa26$^{LSL\text{-}DTA}$ ApoE$^{-/-}$ mice fed a 7-week ND.

A, Representative flow cytometric analysis and quantification of CD4$^+$, CD4$^+$ memory, CD8$^+$ and CD8$^+$ memory T cells in lymph nodes. **B**, Quantification of the frequencies of CD4$^+$, CD8$^+$, CD4$^+$CD69$^+$ and CD8$^+$CD69$^+$ T cells in the lymph nodes. **C**, Representative flow cytometric analysis and quantification of CD4$^+$, CD4$^+$ memory, CD8$^+$ and CD8$^+$ memory T cells in the spleens. **D**, Quantification of the frequencies of CD4$^+$, CD8$^+$, CD4$^+$ CD69$^+$ and CD8$^+$ CD69$^+$ T cells in the spleens. **E** and **F**, Quantification of the numbers of CD4$^+$ and CD8$^+$ T cells in the lymph nodes and spleens. ApoE$^{-/-}$ mice and Xcr1$^{Cre\text{-}Gfp}$ Rosa26$^{LSL\text{-}DTA}$ ApoE$^{-/-}$ mice fed with a 7-week ND (n = 6). Data represent the mean ± SEM. * P<0.05, ** P<0.01, NS, non-significant.

Figure S7. Depletion of Xcr1^{+} cDC1 cells of bone marrow reduces cDC1 cells without affecting macrophages in atherosclerotic lesion of ApoE$^{-/-}$ mice.

A, Diagram of the bone marrow transfer process. ApoE$^{-/-}$ mice transplanted with bone marrow from WT or Xcr1$^{Cre\text{-}Gfp}$ Rosa26$^{LSL\text{-}DTA}$ donors (n = 7). **B**, Body weight of each group. **C**, Serum concentrations of TC, TG, LDL and HDL. **D**, Representative ORO staining images of liver sections and quantification of the ORO positive area percentage in the liver. Scale bar, 50 μm. **E**, Representative flow cytometric analysis of pDC, cDC1 and cDC2 cells in the aortas, Lin^{-} means CD3^{-}CD19^{-}Ly6G^{-}NK1.1^{-}. **F**, Flow cytometric analysis of macrophages in the aortas. Data represent as mean ± SEM. *** P<0.001, NS, non-significant.

Figure S8. The single-cell RNA sequencing process.

Figure S9. Sc-RNA sequencing analysis of the aorta, lymph nodes and spleen in ApoE$^{-/-}$ mice.

A, UMAP plot delineates 10 annotated cell types of Xcr1^{+} cDC1 cells from aorta, lymph node and spleen in ApoE$^{-/-}$ mice maintained on a HFD or ND for 20 weeks. **B-G**, Heatmap statistic map showing marker genes in different clusters. *Ccr7* is the mature gene marker (B). *Sell^{+}CD8a^{-}* cDC1s are defined as Pre-cDC1s (C). *Stmn1* and *Top2a* are the proliferating markers (D). *Itgae* and *Nr4a2* genes marked the transition from early to late immature cDC1s (E). *Cxcl9* and *Cxcl10* genes marked the transition from late immature to early mature cDC1s (F). *Cd63* and *Fscn1* are the late mature markers (G).

Figure S10. Single-cell RNA sequencing of splenic cDC1s from both the HFD and ND groups.

721 **A**, UMAP plot of splenic cDC1s showing annotated clusters. **B**, The proportions of cDC1
722 maturation states across diet groups. **C-H**, Heatmap statistic map depicting representative markers
723 defining cDC1 maturation clusters. *Ccr7* is the mature gene marker (C). *Sell*$^{+}$*CD8a*$^{-}$ cDC1s are
724 defined as Pre-cDC1s (D). *Top2a*, *Stmn1* and *Mki67* are the proliferating markers (E). *Itgae*, *Nr4a2*,
725 *Nr4a3* and *Egr3* genes marked the transition from early to late immature cDC1s (F). *Cxcl9* and
726 *Cxcl10* genes marked the transition from late immature to early mature cDC1s (G). *Cd63* and *Fscn1*
727 are the late mature markers (H). **I-J**, Heatmap statistic map of upregulated genes
728 (*Tnfaip3* and *Serinc3*), and downregulated genes (*Apol7c* and *Tifab*) in the HFD spleen compared
729 to the ND spleen.
730
731 **Figure S11. DC cells analysis in lymph nodes and spleens of ApoE$^{-/-}$ and Xcl1$^{-/-}$ ApoE$^{-/-}$ mice**
732 **fed with 19-week HFD.**
733 **A**, Representative flow cytometric analysis and quantification of pDC, cDCs, cDC1 and cDC2 cells
734 in lymph nodes. **B**, Quantification of absolute counts of pDC, cDCs, cDC1 and cDC2 cells in lymph
735 nodes. **C**, Representative flow cytometric analysis of pDC, cDC1 and cDC2 cells in spleens. **D**,
736 Quantification of absolute counts of pDC, cDCs, cDC1 and cDC2 cells in spleens. ApoE$^{-/-}$ (n = 9)
737 and Xcl1$^{-/-}$ ApoE$^{-/-}$ mice (n = 7 or 8) fed a HFD for 19 weeks. Data represent the mean ± SEM. NS,
738 non-significant.
739
740 **Figure S12. T cells analysis in lymph node and spleen of ApoE$^{-/-}$ and Xcl1$^{-/-}$ ApoE$^{-/-}$ mice fed**
741 **with 16-week HFD.**
742 **A** and **B**, Representative flow cytometric analysis and quantification of absolute counts of CD4^{+},

743 $CD8^+$, $CD4^+CD69^+$ and $CD8^+CD69^+$ T cells in lymph nodes ($ApoE^{-/-}$, n = 9; $Xcl1^{-/-}$ $ApoE^{-/-}$, n =

744 7). **C** and **D**, Representative flow cytometric analysis and quantification of absolute counts of $CD4^+$,

745 $CD8^+$, $CD4^+CD69^+$ and $CD8^+CD69^+$ T cells in spleens ($ApoE^{-/-}$, n = 10; $Xcl1^{-/-}$ $ApoE^{-/-}$, n = 7).

746 Data represent the mean ± SEM. NS, non-significant.

747

748 **Supplementary table 1**: **The top ten high-expressed marker genes in ten clusters**

749

750 **Supplementary table 2**: **Up regulated genes in $Xcr1^+$ cDC1 cells from aorta vs spleen, and**

751 **aorta vs lymph node in ApoE-deficient mice fed a HFD for 20 weeks**

752

753 **Supplementary table 3**: **The sequences of the sgRNA used for generation of $Xcr1^{Cre\text{-}Gfp}$ knock-**

754 **in mice and Xcl1 knockout mice**

755

756 **References**

757 1. Bjorkegren JLM, Lusis AJ. Atherosclerosis: Recent developments. Cell. 2022;185(10):1630-45. doi:
758 10.1016/j.cell.2022.04.004. PubMed PMID: 35504280; PubMed Central PMCID: PMC9119695.
759 2. Hansson GK, Hermansson A. The immune system in atherosclerosis. Nat Immunol.
760 2011;12(3):204-12. Epub 2011/02/16. doi: 10.1038/ni.2001. PubMed PMID: 21321594.
761 3. Lusta KA, Poznyak AV, Sukhorukov VN, Eremin, II, Nadelyaeva, II, Orekhov AN. Hypotheses on
762 Atherogenesis Triggering: Does the Infectious Nature of Atherosclerosis Development Have a
763 Substruction? Cells. 2023;12(5). doi: 10.3390/cells12050707. PubMed PMID: 36899843; PubMed
764 Central PMCID: PMC10001176.
765 4. Hansson GK, Robertson AK, Soderberg-Naucler C. Inflammation and atherosclerosis. Annu Rev
766 Pathol. 2006;1:297-329. Epub 2007/11/28. doi: 10.1146/annurev.pathol.1.110304.100100. PubMed
767 PMID: 18039117.
768 5. Hasham SN, Pillarisetti S. Vascular lipases, inflammation and atherosclerosis. Clin Chim Acta.
769 2006;372(1-2):179-83. Epub 2006/06/13. doi: 10.1016/j.cca.2006.04.020. PubMed PMID: 16765928.
770 6. Steinman RM, Hawiger D, Liu K, Bonifaz L, Bonnyay D, Mahnke K, et al. Dendritic cell function
771 in vivo during the steady state: a role in peripheral tolerance. Ann N Y Acad Sci. 2003;987:15-25. Epub

2003/05/03. doi: 10.1111/j.1749-6632.2003.tb06029.x. PubMed PMID: 12727620.
7. Ma-Krupa W, Jeon MS, Spoerl S, Tedder TF, Goronzy JJ, Weyand CM. Activation of arterial wall dendritic cells and breakdown of self-tolerance in giant cell arteritis. J Exp Med. 2004;199(2):173-83. Epub 2004/01/22. doi: 10.1084/jem.20030850. PubMed PMID: 14734523; PubMed Central PMCID: PMCPMC2211768.
8. Liu P, Yu YR, Spencer JA, Johnson AE, Vallanat CT, Fong AM, et al. CX3CR1 deficiency impairs dendritic cell accumulation in arterial intima and reduces atherosclerotic burden. Arterioscler Thromb Vasc Biol. 2008;28(2):243-50. Epub 2007/12/15. doi: 10.1161/ATVBAHA.107.158675. PubMed PMID: 18079406.
9. Jongstra-Bilen J, Haidari M, Zhu SN, Chen M, Guha D, Cybulsky MI. Low-grade chronic inflammation in regions of the normal mouse arterial intima predisposed to atherosclerosis. J Exp Med. 2006;203(9):2073-83. Epub 2006/08/09. doi: 10.1084/jem.20060245. PubMed PMID: 16894012; PubMed Central PMCID: PMCPMC2118407.
10. Bobryshev YV, Lord RS. Ultrastructural recognition of cells with dendritic cell morphology in human aortic intima. Contacting interactions of Vascular Dendritic Cells in athero-resistant and athero-prone areas of the normal aorta. Arch Histol Cytol. 1995;58(3):307-22. Epub 1995/08/01. doi: 10.1679/aohc.58.307. PubMed PMID: 8527238.
11. Kawahara I, Kitagawa N, Tsutsumi K, Nagata I, Hayashi T, Koji T. The expression of vascular dendritic cells in human atherosclerotic carotid plaques. Hum Pathol. 2007;38(9):1378-85. Epub 2007/06/09. doi: 10.1016/j.humpath.2007.02.004. PubMed PMID: 17555794.
12. Zernecke A, Erhard F, Weinberger T, Schulz C, Ley K, Saliba AE, et al. Integrated single-cell analysis based classification of vascular mononuclear phagocytes in mouse and human atherosclerosis. Cardiovasc Res. 2022. Epub 2022/10/04. doi: 10.1093/cvr/cvac161. PubMed PMID: 36190844.
13. Eisenbarth SC. Dendritic cell subsets in T cell programming: location dictates function. Nat Rev Immunol. 2019;19(2):89-103. Epub 2018/11/23. doi: 10.1038/s41577-018-0088-1. PubMed PMID: 30464294; PubMed Central PMCID: PMCPMC7755085.
14. Bayerl F, Meiser P, Donakonda S, Hirschberger A, Lacher SB, Pedde AM, et al. Tumor-derived prostaglandin E2 programs cDC1 dysfunction to impair intratumoral orchestration of anti-cancer T cell responses. Immunity. 2023;56(6):1341-58 e11. Epub 2023/06/15. doi: 10.1016/j.immuni.2023.05.011. PubMed PMID: 37315536.
15. Legein B, Janssen EM, Theelen TL, Gijbels MJ, Walraven J, Klarquist JS, et al. Ablation of CD8alpha(+) dendritic cell mediated cross-presentation does not impact atherosclerosis in hyperlipidemic mice. Scientific reports. 2015;5:15414. Epub 20151021. doi: 10.1038/srep15414. PubMed PMID: 26486587; PubMed Central PMCID: PMCPMC4614009.
16. Gil-Pulido J, Cochain C, Lippert MA, Schneider N, Butt E, Amezaga N, et al. Deletion of Batf3-dependent antigen-presenting cells does not affect atherosclerotic lesion formation in mice. PLoS One. 2017;12(8):e0181947. Epub 20170803. doi: 10.1371/journal.pone.0181947. PubMed PMID: 28771609; PubMed Central PMCID: PMCPMC5542449.
17. Choi JH, Cheong C, Dandamudi DB, Park CG, Rodriguez A, Mehandru S, et al. Flt3 signaling-dependent dendritic cells protect against atherosclerosis. Immunity. 2011;35(5):819-31. Epub 2011/11/15. doi: 10.1016/j.immuni.2011.09.014. PubMed PMID: 22078798.
18. Clement M, Haddad Y, Raffort J, Lareyre F, Newland SA, Master L, et al. Deletion of IRF8 (Interferon Regulatory Factor 8)-Dependent Dendritic Cells Abrogates Proatherogenic Adaptive Immunity. Circ Res. 2018;122(6):813-20. Epub 2018/02/14. doi: 10.1161/CIRCRESAHA.118.312713.

PubMed PMID: 29436389.
19. Haddad Y, Lahoute C, Clement M, Laurans L, Metghalchi S, Zeboudj L, et al. The Dendritic Cell Receptor DNGR-1 Promotes the Development of Atherosclerosis in Mice. Circ Res. 2017;121(3):234-43. Epub 2017/06/14. doi: 10.1161/CIRCRESAHA.117.310960. PubMed PMID: 28607102.
20. Wohn C, Le Guen V, Voluzan O, Fiore F, Henri S, Malissen B. Absence of MHC class II on cDC1 dendritic cells triggers fatal autoimmunity to a cross-presented self-antigen. Sci Immunol. 2020;5(45). Epub 2020/03/15. doi: 10.1126/sciimmunol.aba1896. PubMed PMID: 32169954.
21. Mundt S, Mrdjen D, Utz SG, Greter M, Schreiner B, Becher B. Conventional DCs sample and present myelin antigens in the healthy CNS and allow parenchymal T cell entry to initiate neuroinflammation. Sci Immunol. 2019;4(31). doi: 10.1126/sciimmunol.aau8380. PubMed PMID: 30679199.
22. Robbins CS, Hilgendorf I, Weber GF, Theurl I, Iwamoto Y, Figueiredo JL, et al. Local proliferation dominates lesional macrophage accumulation in atherosclerosis. Nat Med. 2013;19(9):1166-72. Epub 2013/08/13. doi: 10.1038/nm.3258. PubMed PMID: 23933982; PubMed Central PMCID: PMCPMC3769444.
23. Potteaux S, Gautier EL, Hutchison SB, van Rooijen N, Rader DJ, Thomas MJ, et al. Suppressed monocyte recruitment drives macrophage removal from atherosclerotic plaques of Apoe-/- mice during disease regression. J Clin Invest. 2011;121(5):2025-36. Epub 2011/04/21. doi: 10.1172/JCI43802. PubMed PMID: 21505265; PubMed Central PMCID: PMCPMC3083793.
24. Yilmaz A, Weber J, Cicha I, Stumpf C, Klein M, Raithel D, et al. Decrease in circulating myeloid dendritic cell precursors in coronary artery disease. J Am Coll Cardiol. 2006;48(1):70-80. Epub 2006/07/04. doi: 10.1016/j.jacc.2006.01.078. PubMed PMID: 16814651.
25. Alberts-Grill N, Denning TL, Rezvan A, Jo H. The role of the vascular dendritic cell network in atherosclerosis. Am J Physiol Cell Physiol. 2013;305(1):C1-21. Epub 2013/04/05. doi: 10.1152/ajpcell.00017.2013. PubMed PMID: 23552284; PubMed Central PMCID: PMCPMC3725520.
26. Yan Y, Thakur M, van der Vorst EPC, Weber C, Doring Y. Targeting the chemokine network in atherosclerosis. Atherosclerosis. 2021;330:95-106. Epub 2021/07/13. doi: 10.1016/j.atherosclerosis.2021.06.912. PubMed PMID: 34247863.
27. Eickhoff S, Brewitz A, Gerner MY, Klauschen F, Komander K, Hemmi H, et al. Robust Anti-viral Immunity Requires Multiple Distinct T Cell-Dendritic Cell Interactions. Cell. 2015;162(6):1322-37. Epub 2015/08/25. doi: 10.1016/j.cell.2015.08.004. PubMed PMID: 26296422; PubMed Central PMCID: PMCPMC4567961.
28. Weber C, Zernecke A, Libby P. The multifaceted contributions of leukocyte subsets to atherosclerosis: lessons from mouse models. Nat Rev Immunol. 2008;8(10):802-15. Epub 2008/10/01. doi: 10.1038/nri2415. PubMed PMID: 18825131.
29. Worbs T, Hammerschmidt SI, Forster R. Dendritic cell migration in health and disease. Nat Rev Immunol. 2017;17(1):30-48. Epub 2016/11/29. doi: 10.1038/nri.2016.116. PubMed PMID: 27890914.
30. Li T, Safitri M, Zhang K, Wang Y, Huang L, Zhu Y, et al. Downregulation of G3BP2 reduces atherosclerotic lesions in ApoE(-/-) mice. Atherosclerosis. 2020;310:64-74. Epub 2020/09/13. doi: 10.1016/j.atherosclerosis.2020.08.003. PubMed PMID: 32919187.
31. Mattiuz R, Wohn C, Ghilas S, Ambrosini M, Alexandre YO, Sanchez C, et al. Novel Cre-Expressing Mouse Strains Permitting to Selectively Track and Edit Type 1 Conventional Dendritic Cells Facilitate Disentangling Their Complexity in vivo. Front Immunol. 2018;9:2805. Epub 2018/12/20. doi: 10.3389/fimmu.2018.02805. PubMed PMID: 30564233; PubMed Central PMCID: PMCPMC6288293.

32. Luche H, Weber O, Nageswara Rao T, Blum C, Fehling HJ. Faithful activation of an extra-bright red fluorescent protein in "knock-in" Cre-reporter mice ideally suited for lineage tracing studies. European journal of immunology. 2007;37(1):43-53. Epub 2006/12/16. doi: 10.1002/eji.200636745. PubMed PMID: 17171761.
33. De Meyer GRY, Zurek M, Puylaert P, Martinet W. Programmed death of macrophages in atherosclerosis: mechanisms and therapeutic targets. Nat Rev Cardiol. 2024. Epub 2024/01/02. doi: 10.1038/s41569-023-00957-0. PubMed PMID: 38163815.
34. Yu EPK, Reinhold J, Yu H, Starks L, Uryga AK, Foote K, et al. Mitochondrial Respiration Is Reduced in Atherosclerosis, Promoting Necrotic Core Formation and Reducing Relative Fibrous Cap Thickness. Arterioscler Thromb Vasc Biol. 2017;37(12):2322-32. Epub 2017/10/04. doi: 10.1161/ATVBAHA.117.310042. PubMed PMID: 28970293; PubMed Central PMCID: PMCPMC5701734.
35. Piedrahita JA, Zhang SH, Hagaman JR, Oliver PM, Maeda N. Generation of mice carrying a mutant apolipoprotein E gene inactivated by gene targeting in embryonic stem cells. Proc Natl Acad Sci U S A. 1992;89(10):4471-5. Epub 1992/05/15. doi: 10.1073/pnas.89.10.4471. PubMed PMID: 1584779; PubMed Central PMCID: PMCPMC49104.
36. Plump AS, Smith JD, Hayek T, Aalto-Setala K, Walsh A, Verstuyft JG, et al. Severe hypercholesterolemia and atherosclerosis in apolipoprotein E-deficient mice created by homologous recombination in ES cells. Cell. 1992;71(2):343-53. Epub 1992/10/16. doi: 10.1016/0092-8674(92)90362-g. PubMed PMID: 1423598.
37. Fernandez DM, Rahman AH, Fernandez NF, Chudnovskiy A, Amir ED, Amadori L, et al. Single-cell immune landscape of human atherosclerotic plaques. Nat Med. 2019;25(10):1576-88. Epub 2019/10/09. doi: 10.1038/s41591-019-0590-4. PubMed PMID: 31591603; PubMed Central PMCID: PMCPMC7318784.
38. Afek A, Harats D, Roth A, Keren G, George J. Evidence for the involvement of T cell costimulation through the B-7/CD28 pathway in atherosclerotic plaques from apolipoprotein E knockout mice. Exp Mol Pathol. 2004;76(3):219-23. Epub 2004/05/06. doi: 10.1016/j.yexmp.2003.12.001. PubMed PMID: 15126104.
39. Cancel JC, Crozat K, Dalod M, Mattiuz R. Are Conventional Type 1 Dendritic Cells Critical for Protective Antitumor Immunity and How? Front Immunol. 2019;10:9. Epub 2019/02/28. doi: 10.3389/fimmu.2019.00009. PubMed PMID: 30809220; PubMed Central PMCID: PMCPMC6379659.
40. Li N, Steiger S, Fei L, Li C, Shi C, Salei N, et al. IRF8-Dependent Type I Conventional Dendritic Cells (cDC1s) Control Post-Ischemic Inflammation and Mildly Protect Against Post-Ischemic Acute Kidney Injury and Disease. Front Immunol. 2021;12:685559. Epub 2021/07/09. doi: 10.3389/fimmu.2021.685559. PubMed PMID: 34234783; PubMed Central PMCID: PMCPMC8255684.
41. Bosteels V, Marechal S, De Nolf C, Rennen S, Maelfait J, Tavernier SJ, et al. LXR signaling controls homeostatic dendritic cell maturation. Sci Immunol. 2023;8(83):eadd3955. Epub 2023/05/12. doi: 10.1126/sciimmunol.add3955. PubMed PMID: 37172103.
42. Bottcher JP, Bonavita E, Chakravarty P, Blees H, Cabeza-Cabrerizo M, Sammicheli S, et al. NK Cells Stimulate Recruitment of cDC1 into the Tumor Microenvironment Promoting Cancer Immune Control. Cell. 2018;172(5):1022-37 e14. doi: 10.1016/j.cell.2018.01.004. PubMed PMID: 29429633; PubMed Central PMCID: PMC5847168.
43. Dorner BG, Dorner MB, Zhou X, Opitz C, Mora A, Guttler S, et al. Selective expression of the chemokine receptor XCR1 on cross-presenting dendritic cells determines cooperation with CD8+ T cells.

Immunity. 2009;31(5):823-33. doi: 10.1016/j.immuni.2009.08.027. PubMed PMID: 19913446.
44. Xu F, He D, Ning R, Zeng B, Thompson CW, Li Y, et al. Genetic diversity of chemokine XCL1 and its receptor XCR1 in murine rodents. Developmental and comparative immunology. 2019;98:80-8. doi: 10.1016/j.dci.2019.04.008. PubMed PMID: 31026469.
45. Yoshida T, Izawa D, Nakayama T, Nakahara K, Kakizaki M, Imai T, et al. Molecular cloning of mXCR1, the murine SCM-1/lymphotactin receptor. FEBS letters. 1999;458(1):37-40. doi: 10.1016/s0014-5793(99)01114-x. PubMed PMID: 10518929.
46. Tall AR, Bornfeldt KE. Inflammasomes and Atherosclerosis: a Mixed Picture. Circ Res. 2023;132(11):1505-20. doi: 10.1161/CIRCRESAHA.123.321637. PubMed PMID: 37228237; PubMed Central PMCID: PMC10213995.
47. Vallejo J, Cochain C, Zernecke A, Ley K. Heterogeneity of immune cells in human atherosclerosis revealed by scRNA-Seq. Cardiovasc Res. 2021;117(13):2537-43. doi: 10.1093/cvr/cvab260. PubMed PMID: 34343272; PubMed Central PMCID: PMC8921647.
48. Guo X, Zhou Y, Wu T, Zhu X, Lai W, Wu L. Generation of mouse and human dendritic cells in vitro. J Immunol Methods. 2016;432:24-9. Epub 2016/02/16. doi: 10.1016/j.jim.2016.02.011. PubMed PMID: 26876301.
49. Anselmi G, Helft J, Guermonprez P. Development and function of human dendritic cells in humanized mice models. Mol Immunol. 2020;125:151-61. Epub 2020/07/21. doi: 10.1016/j.molimm.2020.07.005. PubMed PMID: 32688117.
50. Blanco P, Palucka AK, Pascual V, Banchereau J. Dendritic cells and cytokines in human inflammatory and autoimmune diseases. Cytokine Growth Factor Rev. 2008;19(1):41-52. Epub 2008/02/09. doi: 10.1016/j.cytogfr.2007.10.004. PubMed PMID: 18258476; PubMed Central PMCID: PMCPMC2413068.
51. Steinman RM. Dendritic cells: understanding immunogenicity. European journal of immunology. 2007;37 Suppl 1:S53-60. Epub 2007/11/01. doi: 10.1002/eji.200737400. PubMed PMID: 17972346.
52. Steinman RM, Adams JC, Cohn ZA. Identification of a novel cell type in peripheral lymphoid organs of mice. IV. Identification and distribution in mouse spleen. J Exp Med. 1975;141(4):804-20. Epub 1975/04/01. PubMed PMID: 1127378; PubMed Central PMCID: PMCPMC2189754.
53. Steinman RM, Kaplan G, Witmer MD, Cohn ZA. Identification of a novel cell type in peripheral lymphoid organs of mice. V. Purification of spleen dendritic cells, new surface markers, and maintenance in vitro. J Exp Med. 1979;149(1):1-16. Epub 1979/01/01. doi: 10.1084/jem.149.1.1. PubMed PMID: 762493; PubMed Central PMCID: PMCPMC2184752.
54. Clark GJ, Silveira PA, Hogarth PM, Hart DNJ. The cell surface phenotype of human dendritic cells. Semin Cell Dev Biol. 2019;86:3-14. Epub 2018/03/03. doi: 10.1016/j.semcdb.2018.02.013. PubMed PMID: 29499385.
55. Brewitz A, Eickhoff S, Dahling S, Quast T, Bedoui S, Kroczek RA, et al. CD8(+) T Cells Orchestrate pDC-XCR1(+) Dendritic Cell Spatial and Functional Cooperativity to Optimize Priming. Immunity. 2017;46(2):205-19. Epub 2017/02/14. doi: 10.1016/j.immuni.2017.01.003. PubMed PMID: 28190711; PubMed Central PMCID: PMCPMC5362251.
56. Alexandre YO, Ghilas S, Sanchez C, Le Bon A, Crozat K, Dalod M. XCR1+ dendritic cells promote memory CD8+ T cell recall upon secondary infections with Listeria monocytogenes or certain viruses. J Exp Med. 2016;213(1):75-92. Epub 2015/12/24. doi: 10.1084/jem.20142350. PubMed PMID: 26694969; PubMed Central PMCID: PMCPMC4710197.
57. Domenjo-Vila E, Casella V, Iwabuchi R, Fossum E, Pedragosa M, Castellvi Q, et al. XCR1+ DCs

are critical for T cell-mediated immunotherapy of chronic viral infections. Cell Rep. 2023;42(2):112123. Epub 2023/02/17. doi: 10.1016/j.celrep.2023.112123. PubMed PMID: 36795562.

58. Deczkowska A, David E, Ramadori P, Pfister D, Safran M, Li B, et al. XCR1(+) type 1 conventional dendritic cells drive liver pathology in non-alcoholic steatohepatitis. Nat Med. 2021;27(6):1043-54. Epub 2021/05/22. doi: 10.1038/s41591-021-01344-3. PubMed PMID: 34017133.

59. Mysore V, Tahir S, Furuhashi K, Arora J, Rosetti F, Cullere X, et al. Monocytes transition to macrophages within the inflamed vasculature via monocyte CCR2 and endothelial TNFR2. J Exp Med. 2022;219(5). Epub 2022/04/12. doi: 10.1084/jem.20210562. PubMed PMID: 35404389; PubMed Central PMCID: PMCPMC9006314.

60. Liu Z, Liao F, Zhu J, Zhou D, Heo GS, Leuhmann HP, et al. Reprogramming alveolar macrophage responses to TGF-beta reveals CCR2+ monocyte activity that promotes bronchiolitis obliterans syndrome. J Clin Invest. 2022;132(19). Epub 2022/10/04. doi: 10.1172/JCI159229. PubMed PMID: 36189800; PubMed Central PMCID: PMCPMC9525120.

61. Kim D, An L, Moon J, Maymi VI, McGurk AI, Rudd BD, et al. Ccr2+ Monocyte-Derived Macrophages Influence Trajectories of Acquired Therapy Resistance in Braf-Mutant Melanoma. Cancer Res. 2023;83(14):2328-44. Epub 2023/05/17. doi: 10.1158/0008-5472.CAN-22-2841. PubMed PMID: 37195124; PubMed Central PMCID: PMCPMC10478295.

62. Liu Z, Gu Y, Chakarov S, Bleriot C, Kwok I, Chen X, et al. Fate Mapping via Ms4a3-Expression History Traces Monocyte-Derived Cells. Cell. 2019;178(6):1509-25.e19. Epub 2019/09/07. doi: 10.1016/j.cell.2019.08.009. PubMed PMID: 31491389.

63. Bosmans LA, van Tiel CM, Aarts S, Willemsen L, Baardman J, van Os BW, et al. Myeloid CD40 deficiency reduces atherosclerosis by impairing macrophages' transition into a pro-inflammatory state. Cardiovasc Res. 2023;119(5):1146-60. Epub 2022/05/20. doi: 10.1093/cvr/cvac084. PubMed PMID: 35587037; PubMed Central PMCID: PMCPMC10202633.

64. Mildner A, Schonheit J, Giladi A, David E, Lara-Astiaso D, Lorenzo-Vivas E, et al. Genomic Characterization of Murine Monocytes Reveals C/EBPbeta Transcription Factor Dependence of Ly6C(-) Cells. Immunity. 2017;46(5):849-62 e7. Epub 2017/05/18. doi: 10.1016/j.immuni.2017.04.018. PubMed PMID: 28514690.

65. Inui H, Nishida M, Ichii M, Nakaoka H, Asaji M, Ide S, et al. XCR1(+) conventional dendritic cell-induced CD4(+) T helper 1 cell activation exacerbates cardiac remodeling after ischemic myocardial injury. J Mol Cell Cardiol. 2023;176:68-83. Epub 2023/02/06. doi: 10.1016/j.yjmcc.2023.01.011. PubMed PMID: 36739942.

66. Moore KJ, Tabas I. Macrophages in the pathogenesis of atherosclerosis. Cell. 2011;145(3):341-55. Epub 2011/05/03. doi: 10.1016/j.cell.2011.04.005. PubMed PMID: 21529710; PubMed Central PMCID: PMCPMC3111065.

67. Yoshida T, Imai T, Kakizaki M, Nishimura M, Takagi S, Yoshie O. Identification of single C motif-1/lymphotactin receptor XCR1. The Journal of biological chemistry. 1998;273(26):16551-4. doi: 10.1074/jbc.273.26.16551. PubMed PMID: 9632725.

68. de Oliveira CE, Gasparoto TH, Pinheiro CR, Amor NG, Nogueira MRS, Kaneno R, et al. CCR5-Dependent Homing of T Regulatory Cells to the Tumor Microenvironment Contributes to Skin Squamous Cell Carcinoma Development. Mol Cancer Ther. 2017;16(12):2871-80. Epub 2017/09/15. doi: 10.1158/1535-7163.MCT-17-0341. PubMed PMID: 28904130.

69. He F, Wu Z, Liu C, Zhu Y, Zhou Y, Tian E, et al. Targeting BCL9/BCL9L enhances antigen presentation by promoting conventional type 1 dendritic cell (cDC1) activation and tumor infiltration.

Signal Transduct Target Ther. 2024;9(1):139. Epub 2024/05/30. doi: 10.1038/s41392-024-01838-9. PubMed PMID: 38811552; PubMed Central PMCID: PMCPMC11137111.

70. Bottcher JP, Beyer M, Meissner F, Abdullah Z, Sander J, Hochst B, et al. Functional classification of memory CD8(+) T cells by CX3CR1 expression. Nat Commun. 2015;6:8306. Epub 2015/09/26. doi: 10.1038/ncomms9306. PubMed PMID: 26404698; PubMed Central PMCID: PMCPMC4667439.

71. Chu VT, Weber T, Graf R, Sommermann T, Petsch K, Sack U, et al. Efficient generation of Rosa26 knock-in mice using CRISPR/Cas9 in C57BL/6 zygotes. BMC Biotechnol. 2016;16:4. Epub 2016/01/17. doi: 10.1186/s12896-016-0234-4. PubMed PMID: 26772810; PubMed Central PMCID: PMCPMC4715285.

72. Larson MA. Pronuclear Microinjection of One-Cell Embryos. Methods in molecular biology. 2020;2066:27-33. doi: 10.1007/978-1-4939-9837-1_2. PubMed PMID: 31512204.

73. Voisinne G, Kersse K, Chaoui K, Lu L, Chaix J, Zhang L, et al. Quantitative interactomics in primary T cells unveils TCR signal diversification extent and dynamics. Nat Immunol. 2019;20(11):1530-41. Epub 2019/10/09. doi: 10.1038/s41590-019-0489-8. PubMed PMID: 31591574; PubMed Central PMCID: PMCPMC6859066.

74. Huang R, Guo G, Lu L, Fu R, Luo J, Liu Z, et al. The three members of the Vav family proteins form complexes that concur to foam cell formation and atherosclerosis. J Lipid Res. 2019;60(12):2006-19. Epub 2019/10/02. doi: 10.1194/jlr.M094771. PubMed PMID: 31570505; PubMed Central PMCID: PMCPMC6889716.

1013 Figure 1

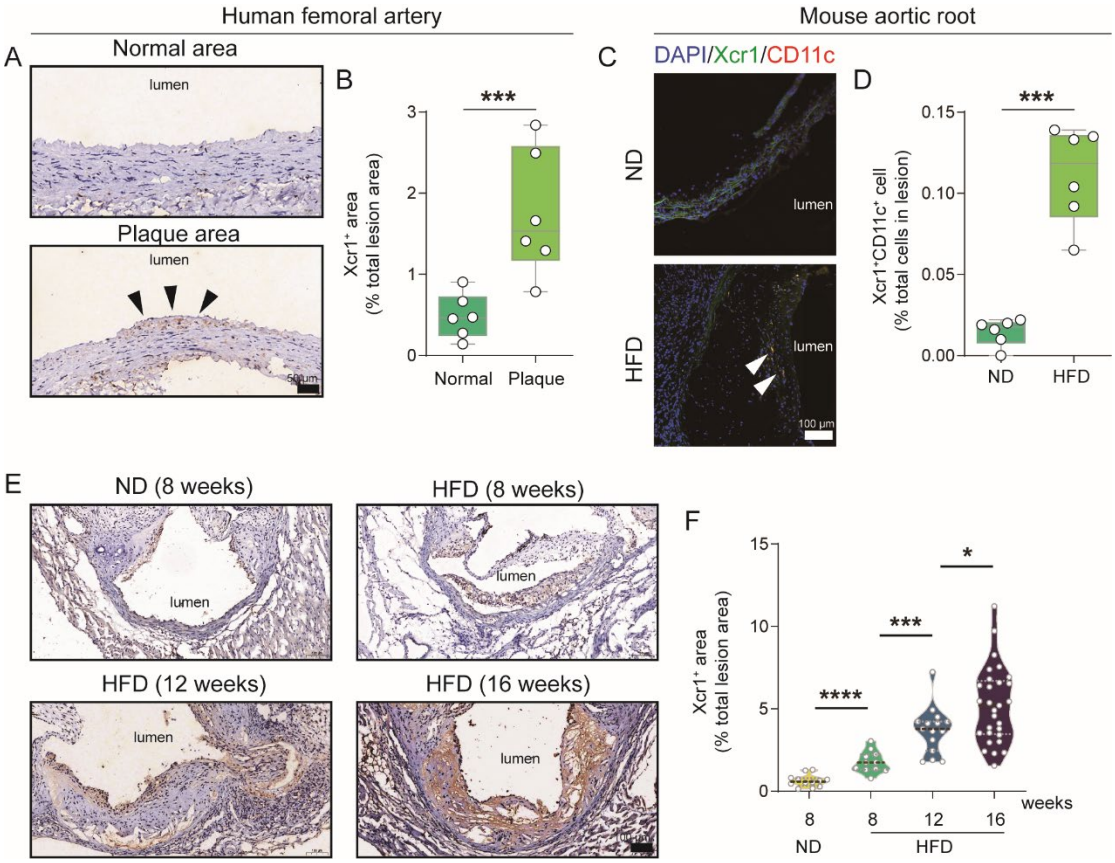

1014

1015

1016 Figure 2

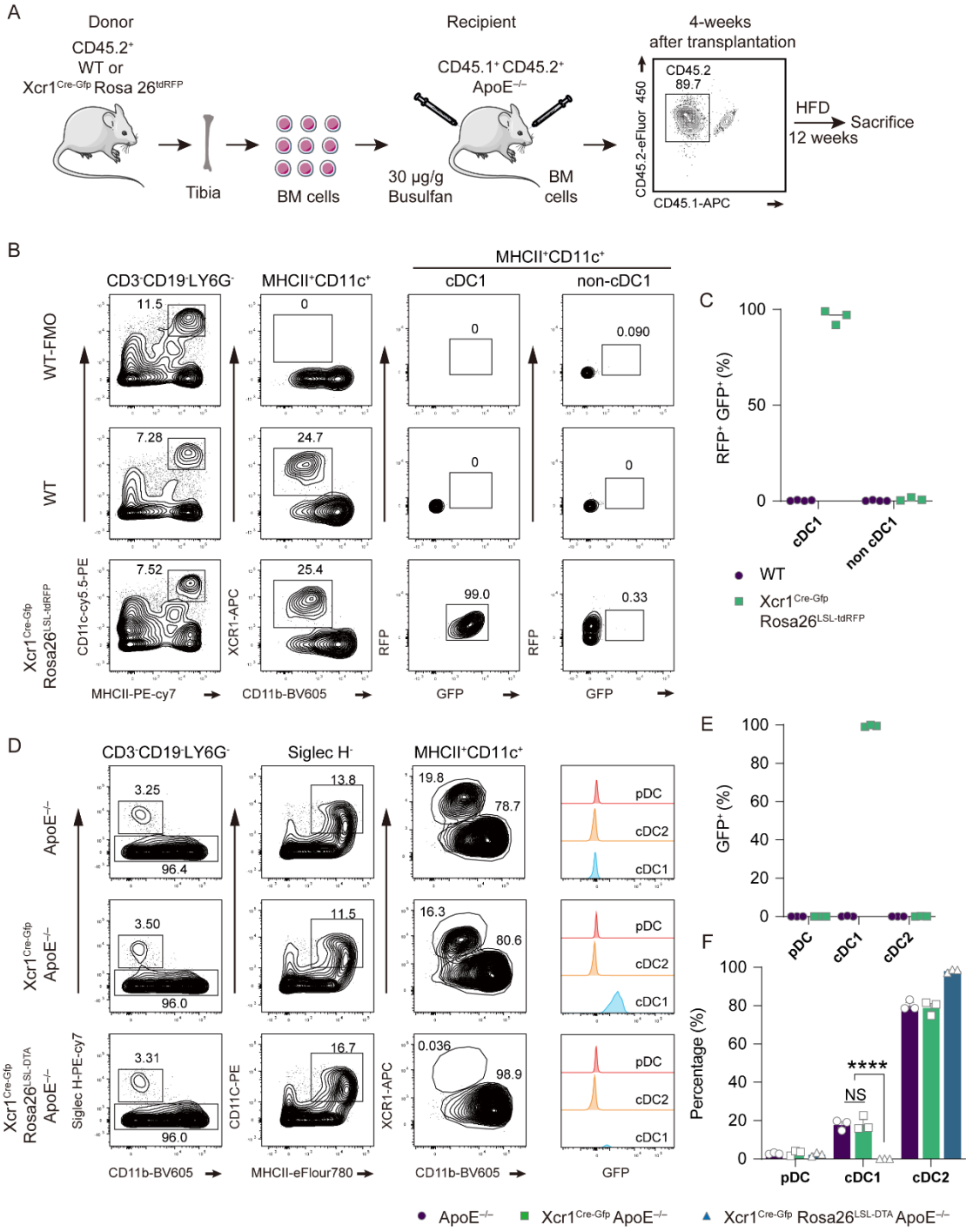

1017
1018

1019 Figure 3

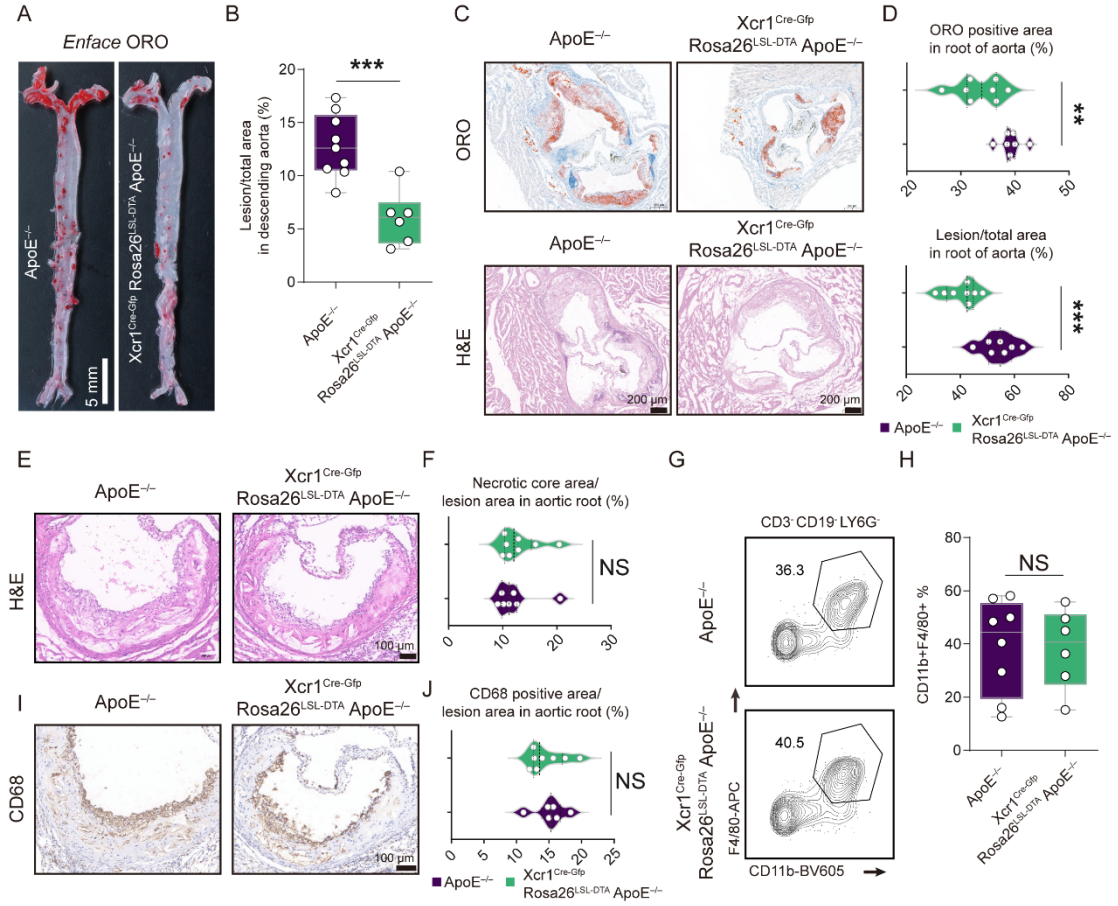

1020
1021

1022 Figure 4

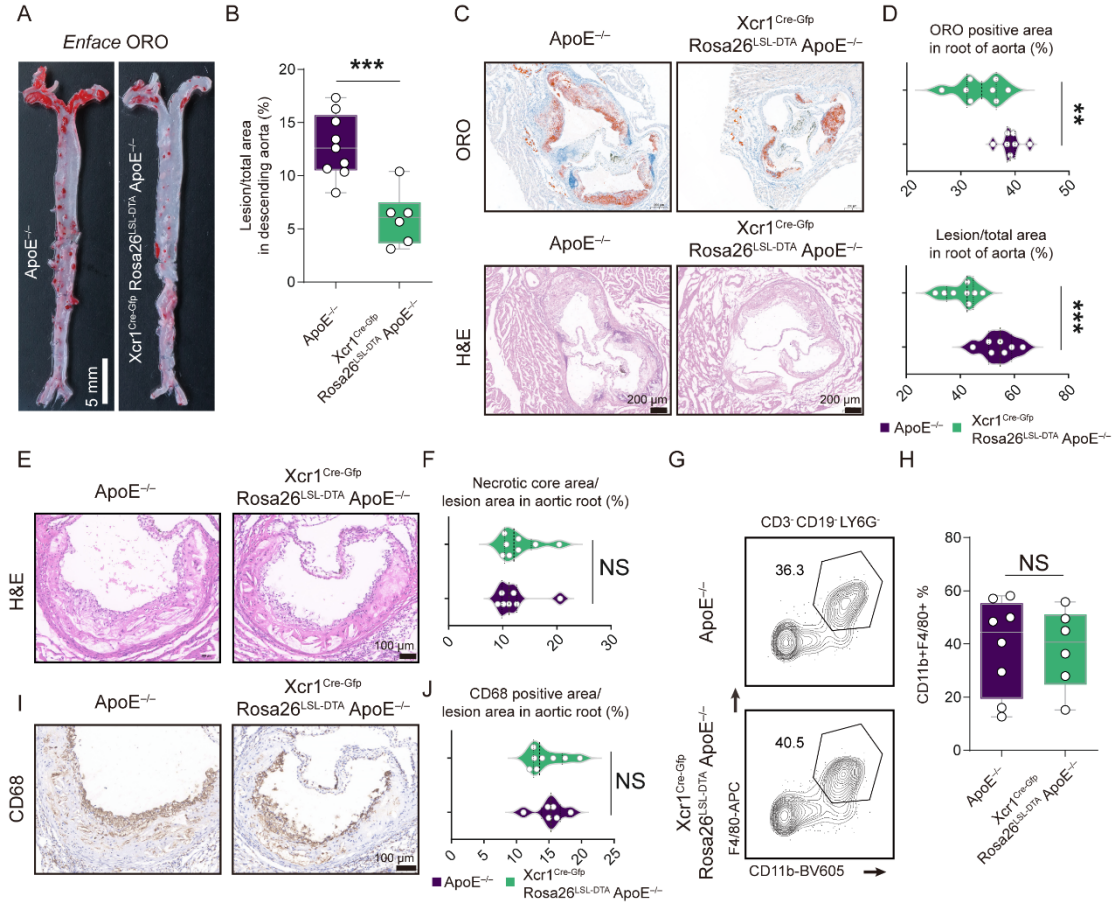

1023
1024

Figure 5

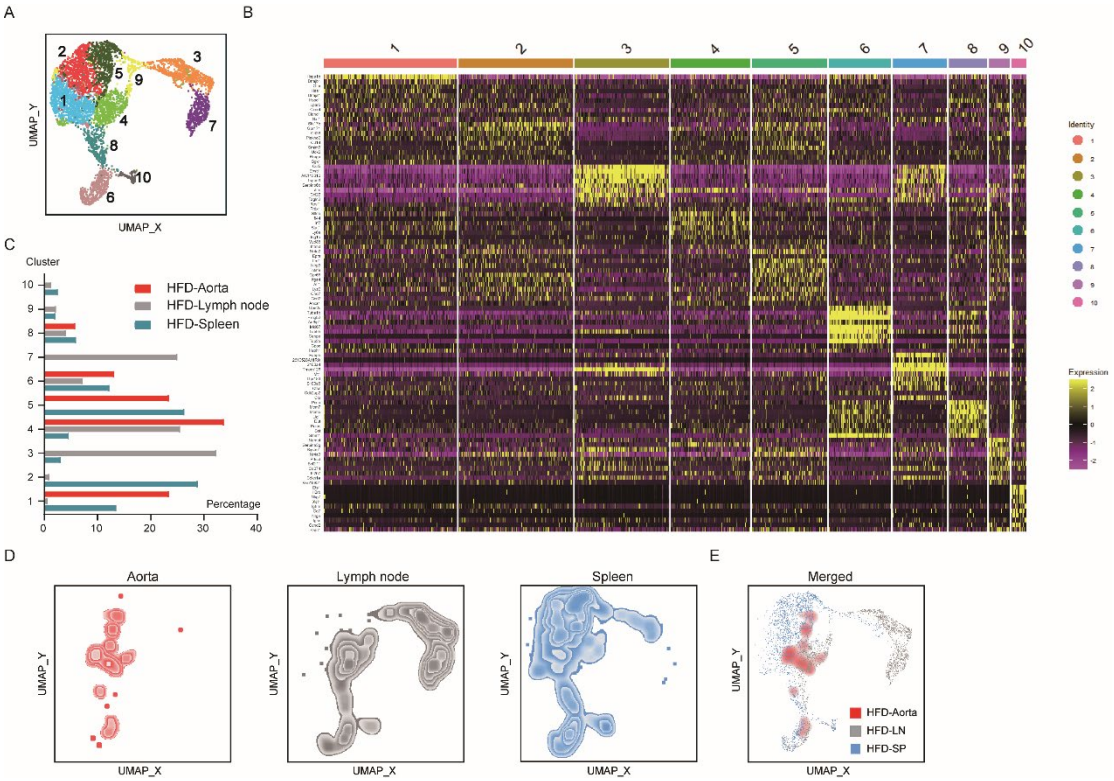
A
B
C
D
E
UMAP_Y
UMAP_X
Cluster
HFD-Aorta
HFD-Lymph node
HFD-Spleen
Percentage
Identity
Expression
Aorta
Lymph node
Spleen
Merged
HFD-Aorta
HFD-LN
HFD-SP

1028 Figure 6

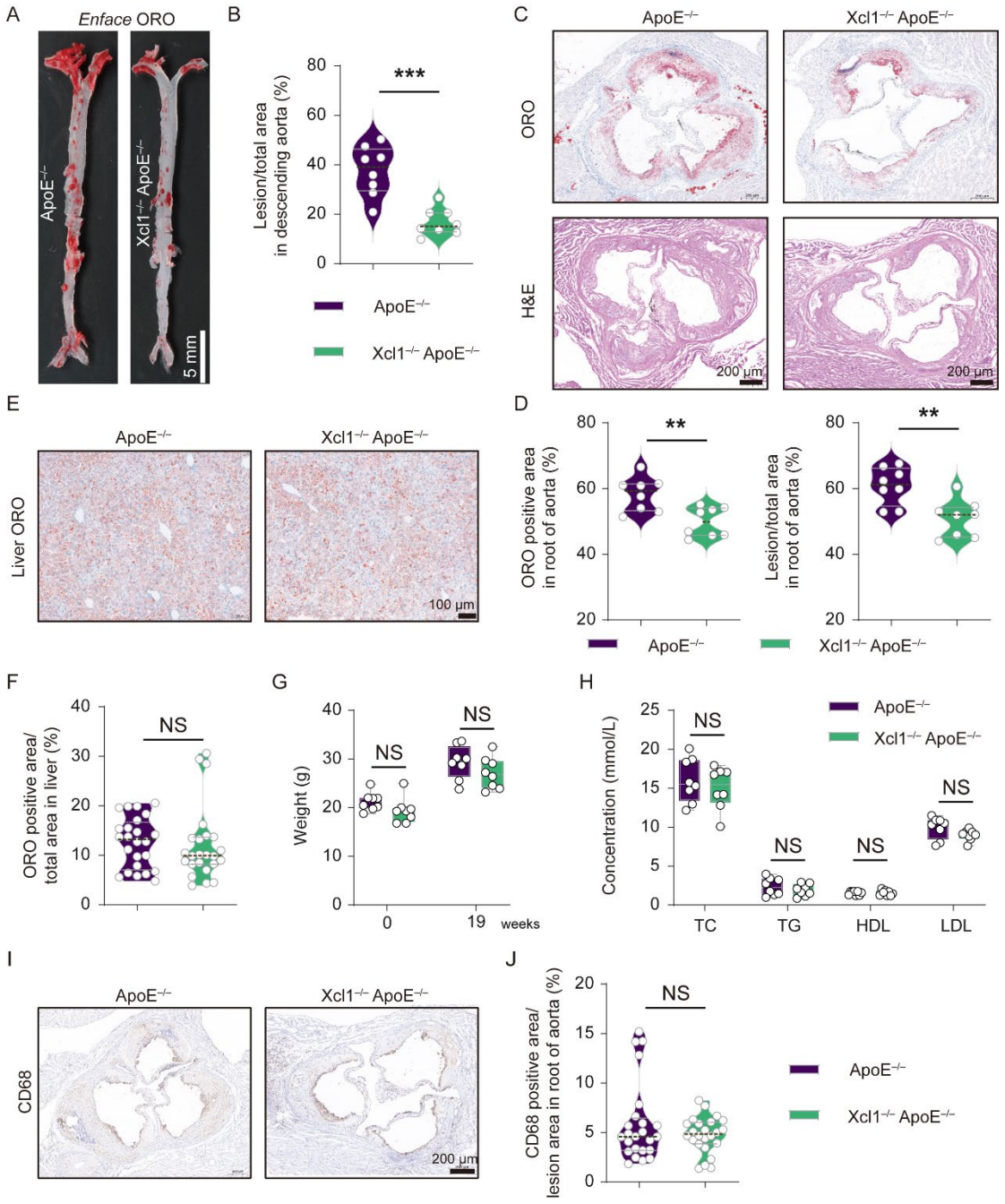

1029

1030

Figure 7

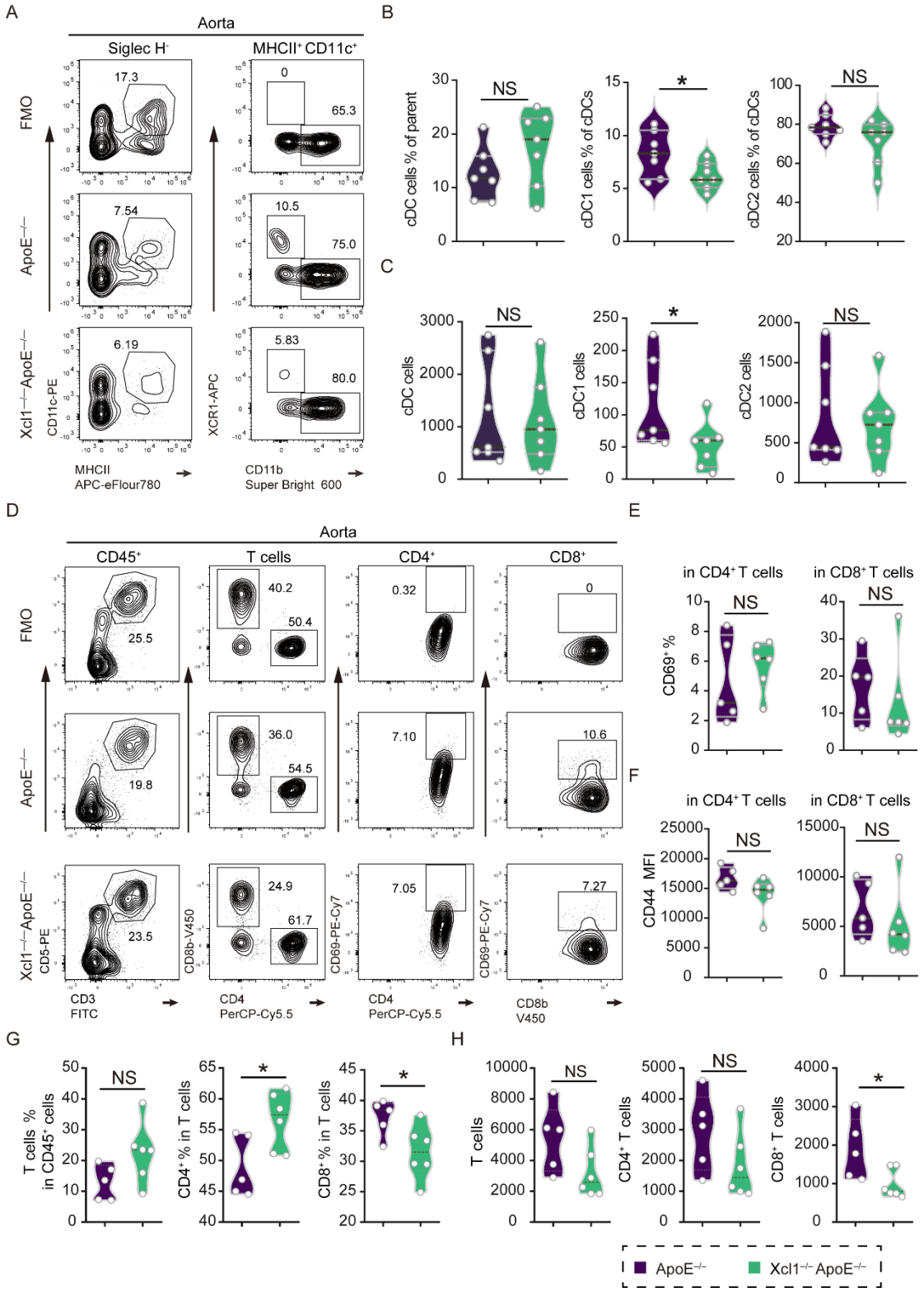
A
Aorta
Siglec H-
MHCII+ CD11c+
FMO
ApoE−/−
Xcl1−/− ApoE−/−
17.3
7.54
6.19
0
65.3
10.5
75.0
5.83
80.0
CD11c-PE
XCR1-APC
MHCII
APC-eFlour780
CD11b
Super Bright 600
B
cDC cells % of parent
cDC1 cells % of cDCs
cDC2 cells % of cDCs
NS
*
NS
C
cDC cells
cDC1 cells
cDC2 cells
NS
*
NS
D
Aorta
CD45+
T cells
CD4+
CD8+
25.5
19.8
23.5
40.2
50.4
36.0
54.5
24.9
61.7
0.32
7.10
7.05
0
10.6
7.27
CD5-PE
CD8b-V450
CD69-PE-Cy7
CD69-PE-Cy7
CD3
FITC
CD4
PerCP-Cy5.5
CD4
PerCP-Cy5.5
CD8b
V450
E
in CD4+ T cells
in CD8+ T cells
CD69+ %
NS
NS
F
in CD4+ T cells
in CD8+ T cells
CD44 MFI
NS
NS
G
T cells % in CD45+ cells
CD4+ % in T cells
CD8+ % in T cells
NS
*
*
H
T cells
CD4+ T cells
CD8+ T cells
NS
NS
*
ApoE−/−
Xcl1−/− ApoE−/−

1034 Figure S1

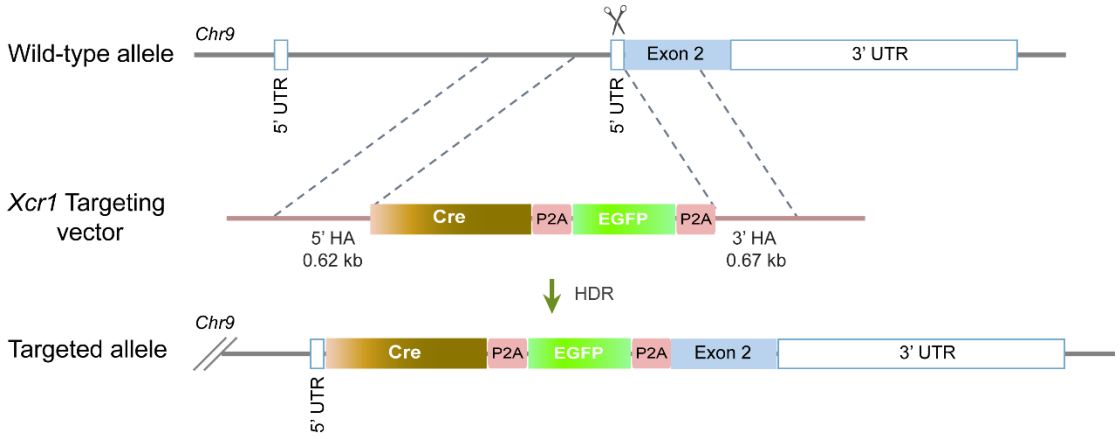

1035

1036

1037 Figure S2

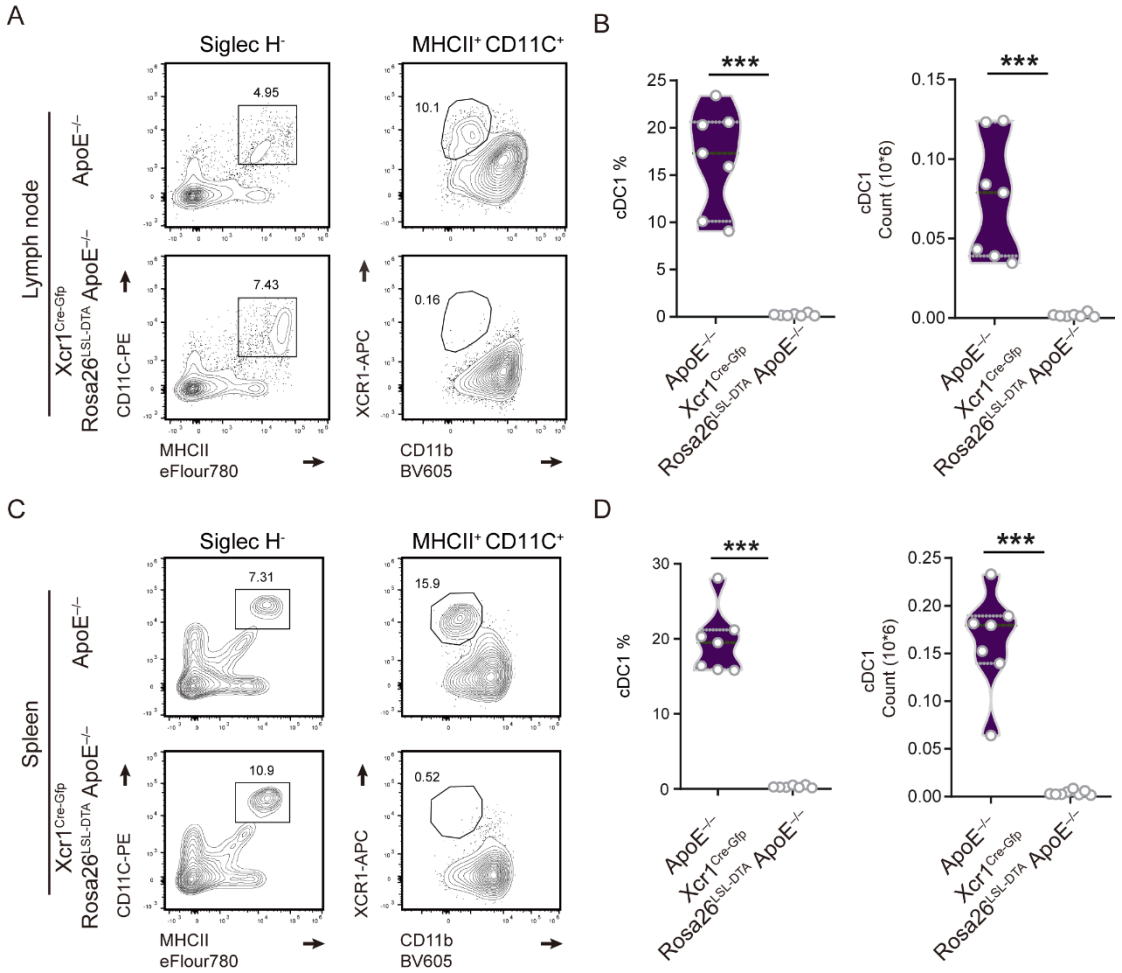

1038

1039

Figure S3

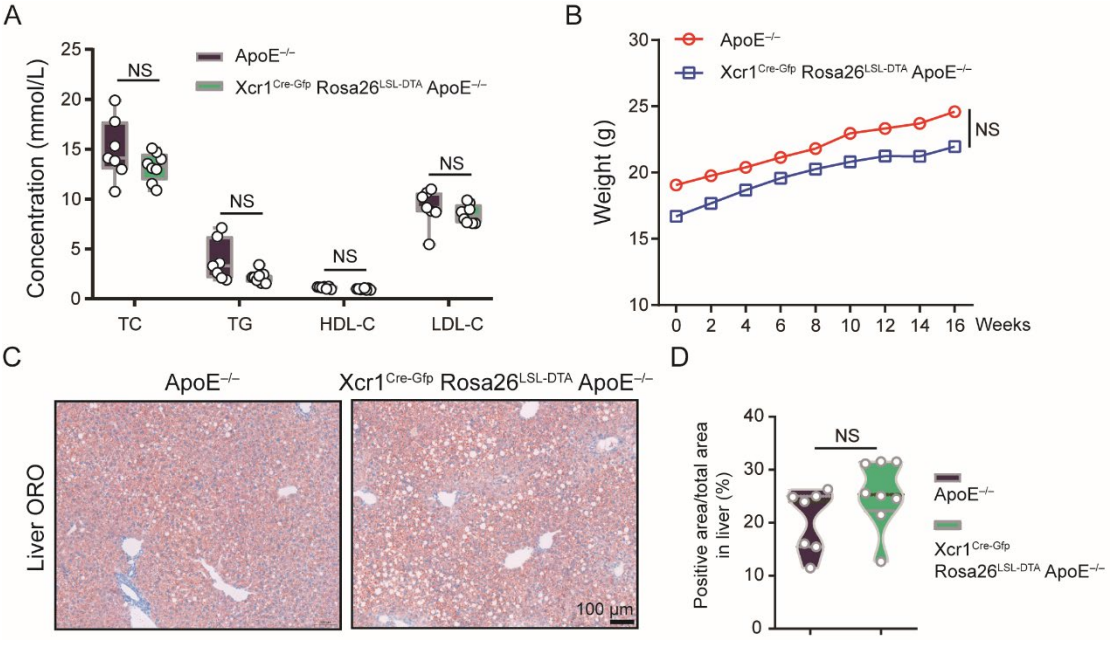
A
Concentration (mmol/L)
ApoE−/−
Xcr1Cre-Gfp Rosa26LSL-DTA ApoE−/−
NS
TC
TG
HDL-C
LDL-C
B
Weight (g)
Weeks
C
Liver ORO
100 μm
D
Positive area/total area in liver (%)

1043 Figure S4

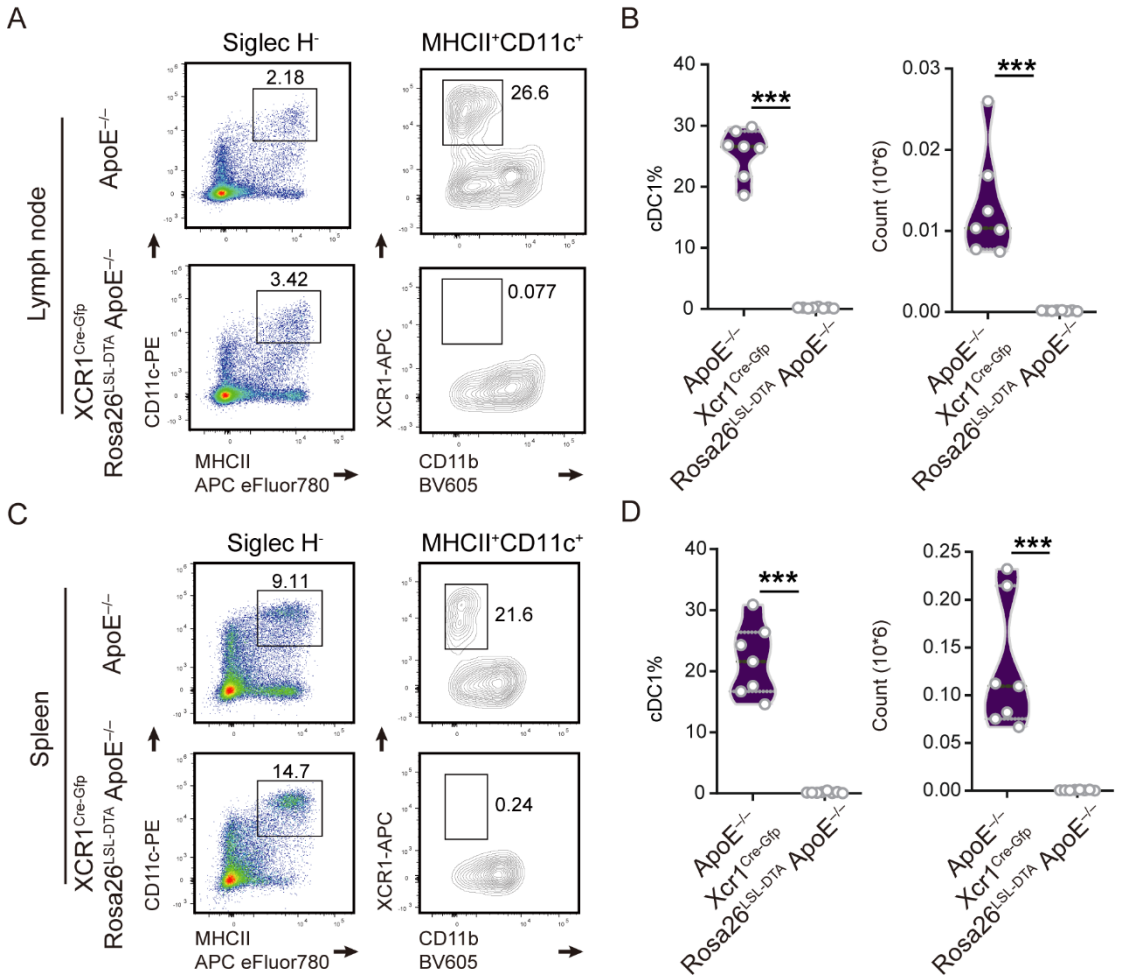

1044

1045

Figure S5

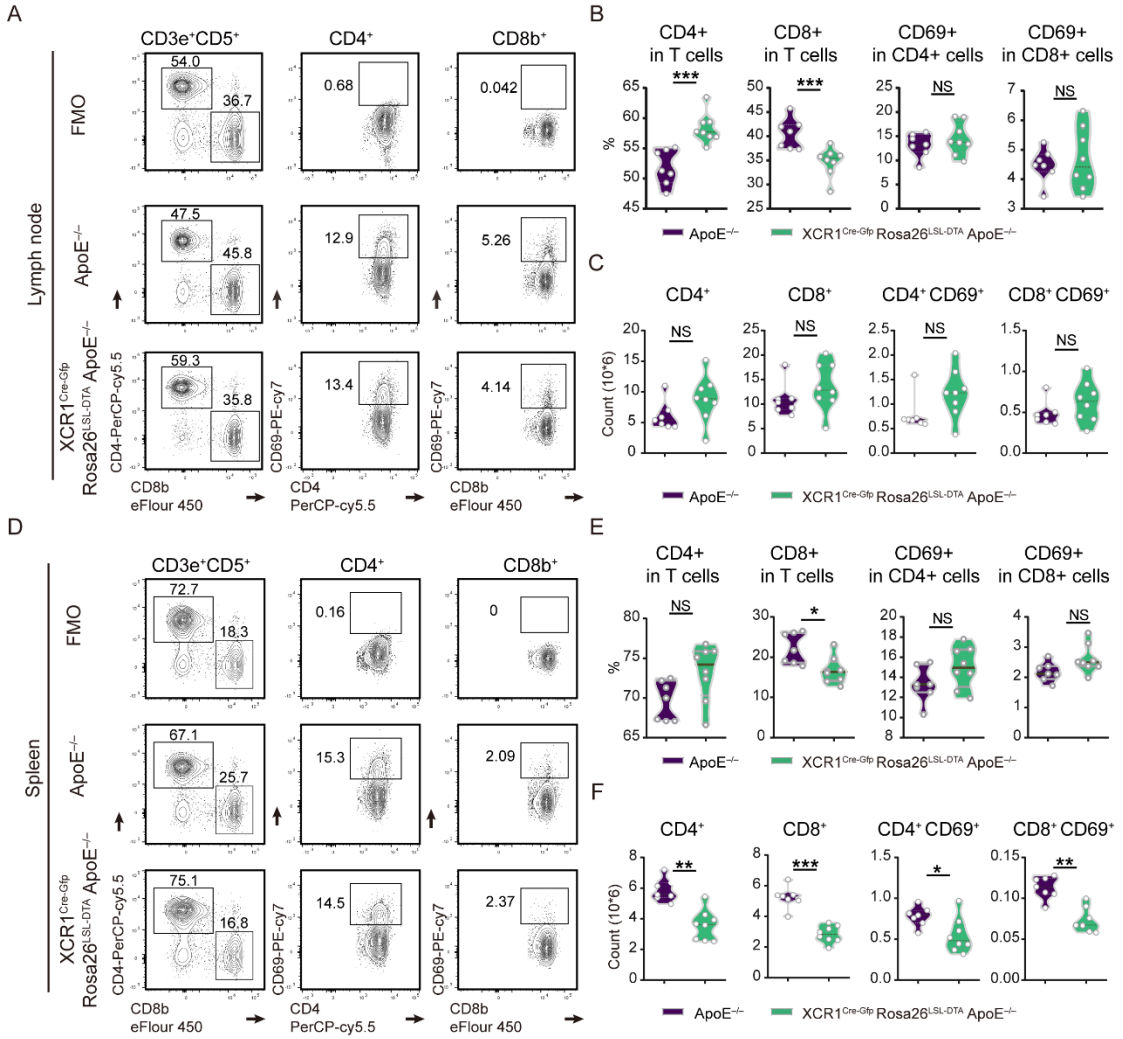
A
Lymph node
FMO
ApoE−/−
XCR1Cre-Gfp Rosa26LSL-DTA ApoE−/−
CD3e+CD5+
CD4+
CD8b+
54.0
36.7
0.68
0.042
47.5
45.8
12.9
5.26
59.3
35.8
13.4
4.14
CD4-PerCP-cy5.5
CD69-PE-cy7
CD8b eFlour 450
CD4 PerCP-cy5.5
B
CD4+ in T cells
CD8+ in T cells
CD69+ in CD4+ cells
CD69+ in CD8+ cells
***
***
NS
NS
%
ApoE−/−
XCR1Cre-Gfp Rosa26LSL-DTA ApoE−/−
C
CD4+
CD8+
CD4+ CD69+
CD8+ CD69+
NS
NS
NS
NS
Count (10*6)
D
Spleen
72.7
18.3
0.16
0
67.1
25.7
15.3
2.09
75.1
16.8
14.5
2.37
E
NS
*
NS
NS
F
**
***
*
**

1049 Figure S6

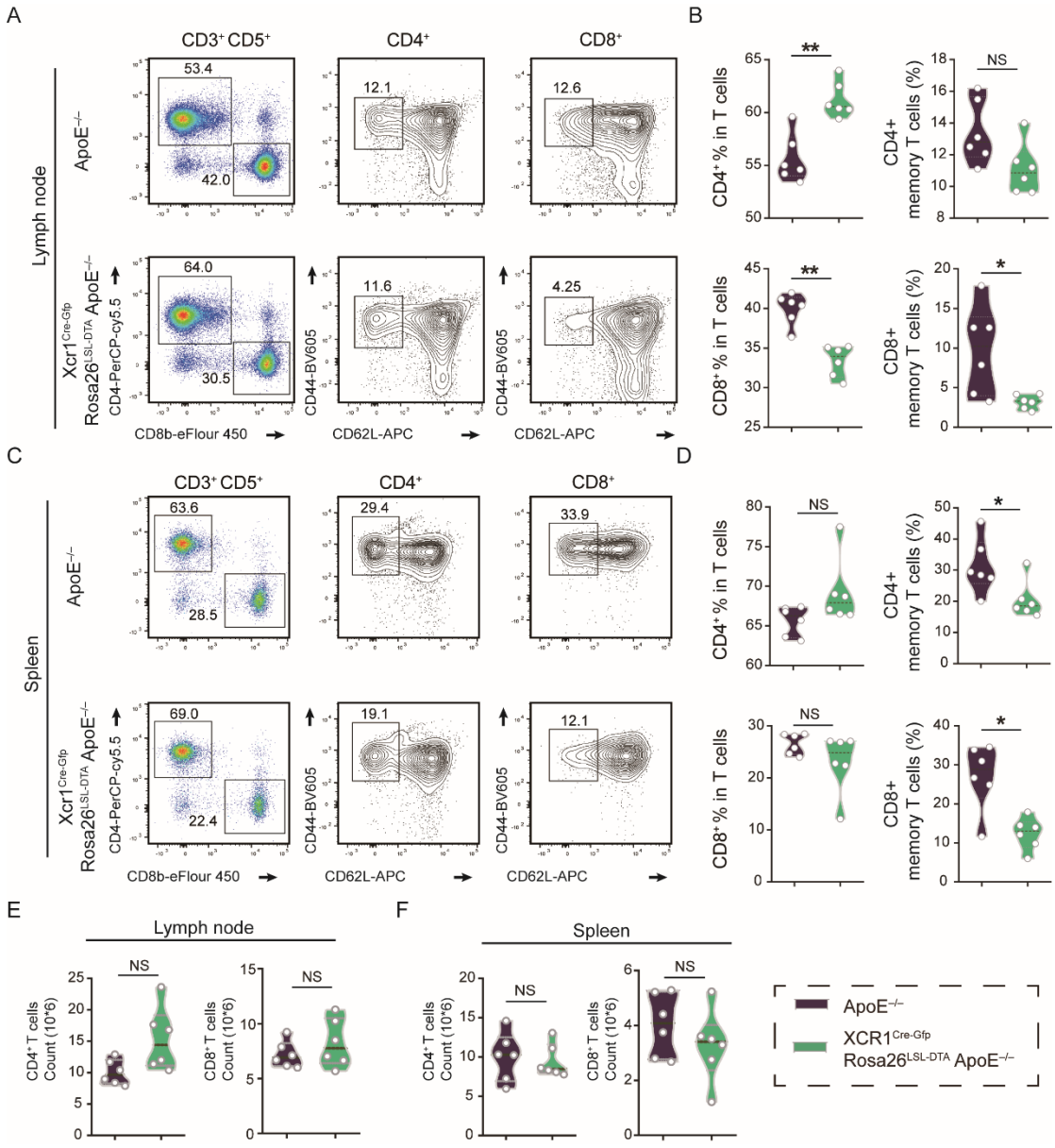

1050

1051

Figure S7

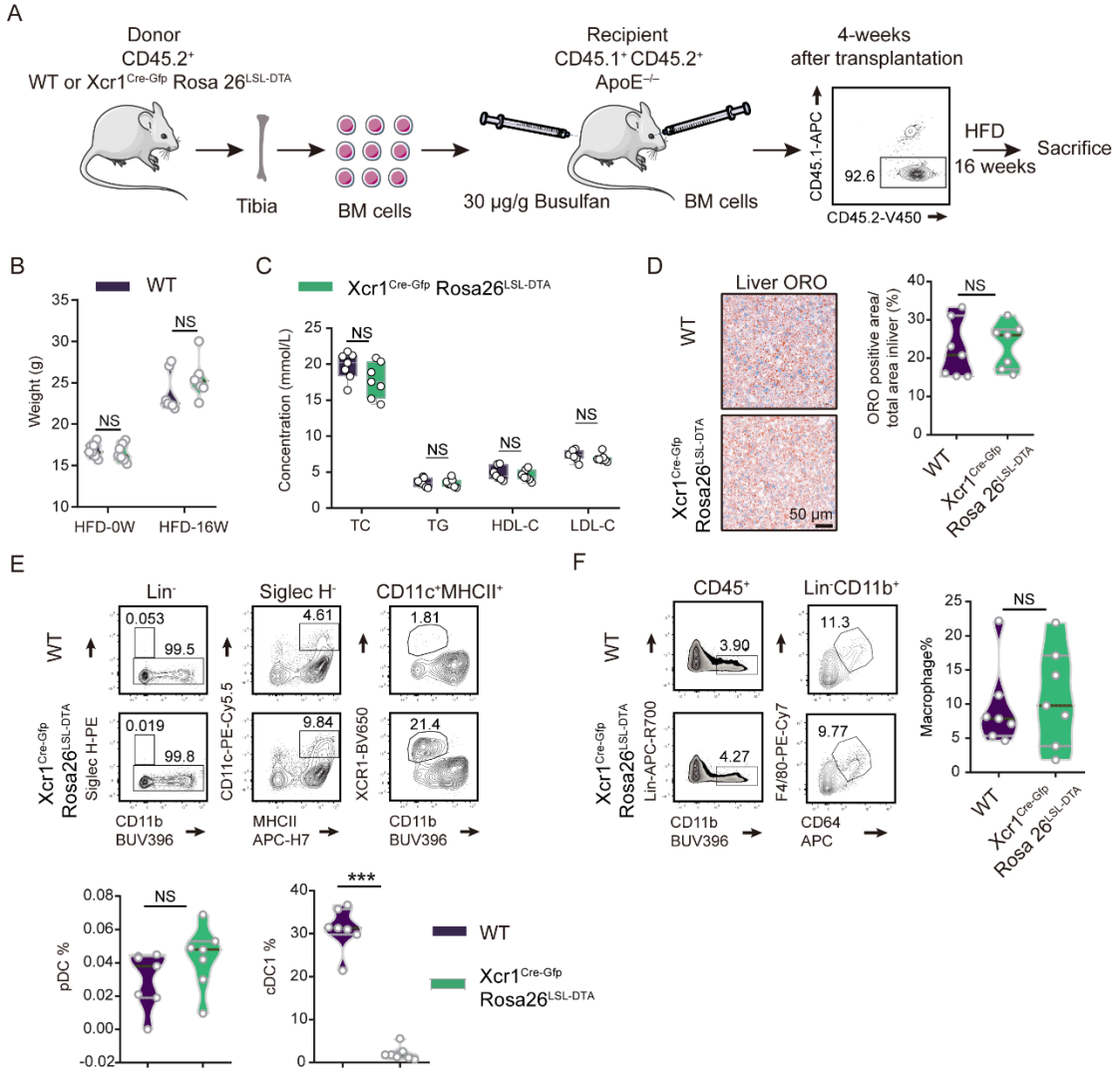
A
Donor
CD45.2+
WT or Xcr1Cre-Gfp Rosa 26LSL-DTA
Tibia
BM cells
30 μg/g Busulfan
Recipient
CD45.1+ CD45.2+
ApoE−/−
BM cells
4-weeks
after transplantation
CD45.1-APC
92.6
CD45.2-V450
HFD
16 weeks
Sacrifice
B
WT
Weight (g)
NS
HFD-0W
HFD-16W
C
Xcr1Cre-Gfp Rosa26LSL-DTA
Concentration (mmol/L)
TC
TG
HDL-C
LDL-C
D
Liver ORO
WT
Xcr1Cre-Gfp Rosa26LSL-DTA
50 μm
ORO positive area/ total area inliver (%)
E
Lin-
Siglec H-
CD11c+MHCII+
0.053
99.5
4.61
1.81
0.019
99.8
9.84
21.4
CD11b BUV396
MHCII APC-H7
CD11b BUV396
Siglec H-PE
CD11c-PE-Cy5.5
XCR1-BV650
pDC %
cDC1 %
***
F
CD45+
Lin-CD11b+
3.90
11.3
4.27
9.77
CD11b BUV396
CD64 APC
Lin-APC-R700
F4/80-PE-Cy7
Macrophage%

Figure S8

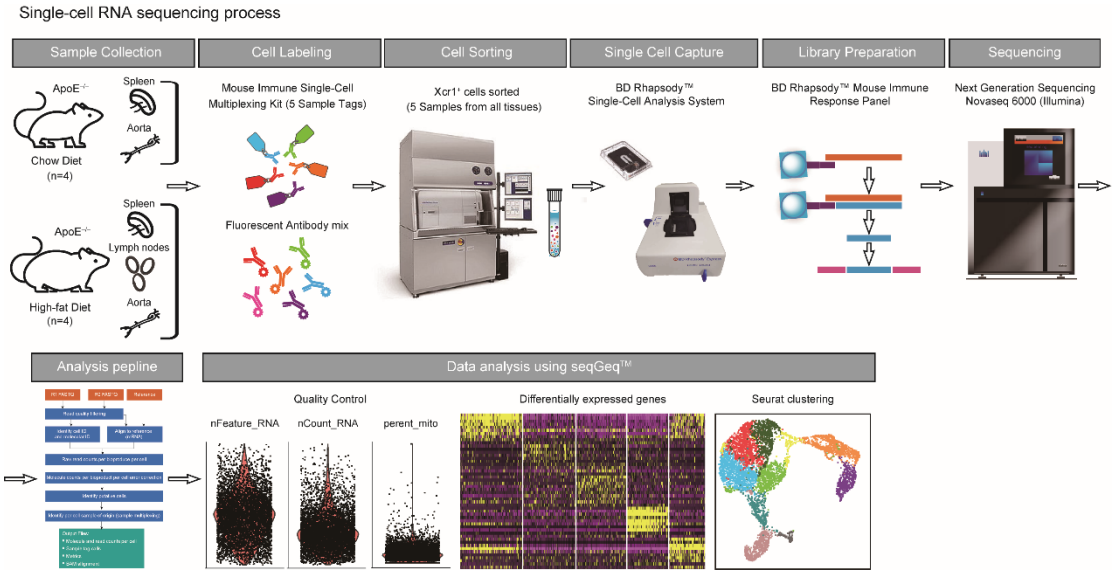
Single-cell RNA sequencing process
Sample Collection
Cell Labeling
Cell Sorting
Single Cell Capture
Library Preparation
Sequencing
ApoE-/-
Spleen
Aorta
Chow Diet
(n=4)
ApoE-/-
Spleen
Lymph nodes
Aorta
High-fat Diet
(n=4)
Mouse Immune Single-Cell Multiplexing Kit (5 Sample Tags)
Fluorescent Antibody mix
Xcr1+ cells sorted
(5 Samples from all tissues)
BD Rhapsody™ Single-Cell Analysis System
BD Rhapsody™ Mouse Immune Response Panel
Next Generation Sequencing Novaseq 6000 (Illumina)
Analysis pepline
Data analysis using seqGeq™
Quality Control
nFeature_RNA
nCount_RNA
perent_mito
Differentially expressed genes
Seurat clustering

Figure S9

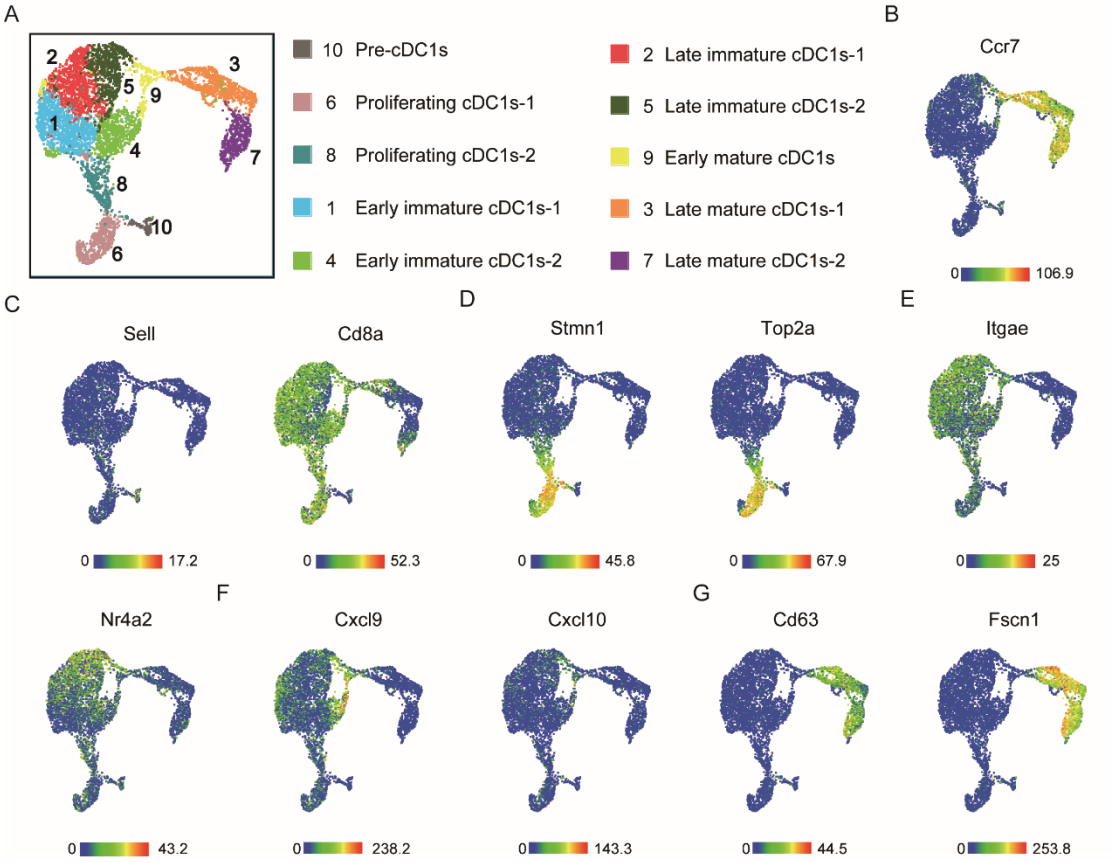
A
10 Pre-cDC1s
6 Proliferating cDC1s-1
8 Proliferating cDC1s-2
1 Early immature cDC1s-1
4 Early immature cDC1s-2
2 Late immature cDC1s-1
5 Late immature cDC1s-2
9 Early mature cDC1s
3 Late mature cDC1s-1
7 Late mature cDC1s-2
B
Ccr7
0 106.9
C
Sell
0 17.2
Cd8a
0 52.3
D
Stmn1
0 45.8
Top2a
0 67.9
E
Itgae
0 25
F
Nr4a2
0 43.2
Cxcl9
0 238.2
Cxcl10
0 143.3
G
Cd63
0 44.5
Fscn1
0 253.8

Figure S10

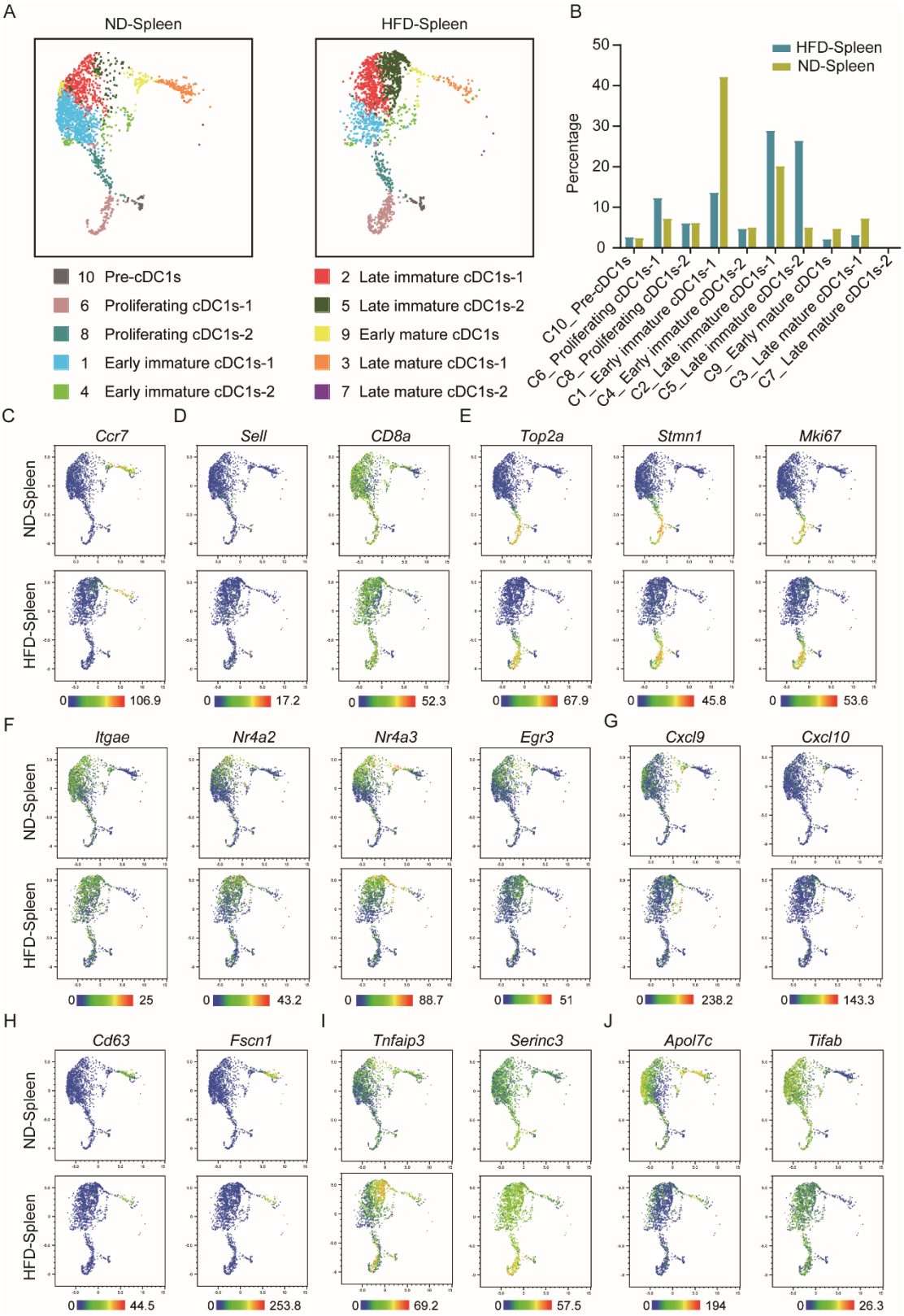
A
ND-Spleen
HFD-Spleen
10 Pre-cDC1s
6 Proliferating cDC1s-1
8 Proliferating cDC1s-2
1 Early immature cDC1s-1
4 Early immature cDC1s-2
2 Late immature cDC1s-1
5 Late immature cDC1s-2
9 Early mature cDC1s
3 Late mature cDC1s-1
7 Late mature cDC1s-2
B
HFD-Spleen
ND-Spleen
Percentage
C10_ Pre-cDC1s
C6_ Proliferating cDC1s-1
C8_ Proliferating cDC1s-2
C1_ Early immature cDC1s-1
C4_ Early immature cDC1s-2
C2_ Late immature cDC1s-1
C5_ Late immature cDC1s-2
C9_ Early mature cDC1s
C3_ Late mature cDC1s-1
C7_ Late mature cDC1s-2
C
D
E
Ccr7
Sell
CD8a
Top2a
Stmn1
Mki67
ND-Spleen
HFD-Spleen
0 106.9
0 17.2
0 52.3
0 67.9
0 45.8
0 53.6
F
G
Itgae
Nr4a2
Nr4a3
Egr3
Cxcl9
Cxcl10
0 25
0 43.2
0 88.7
0 51
0 238.2
0 143.3
H
I
J
Cd63
Fscn1
Tnfaip3
Serinc3
Apol7c
Tifab
0 44.5
0 253.8
0 69.2
0 57.5
0 194
0 26.3

Figure S11

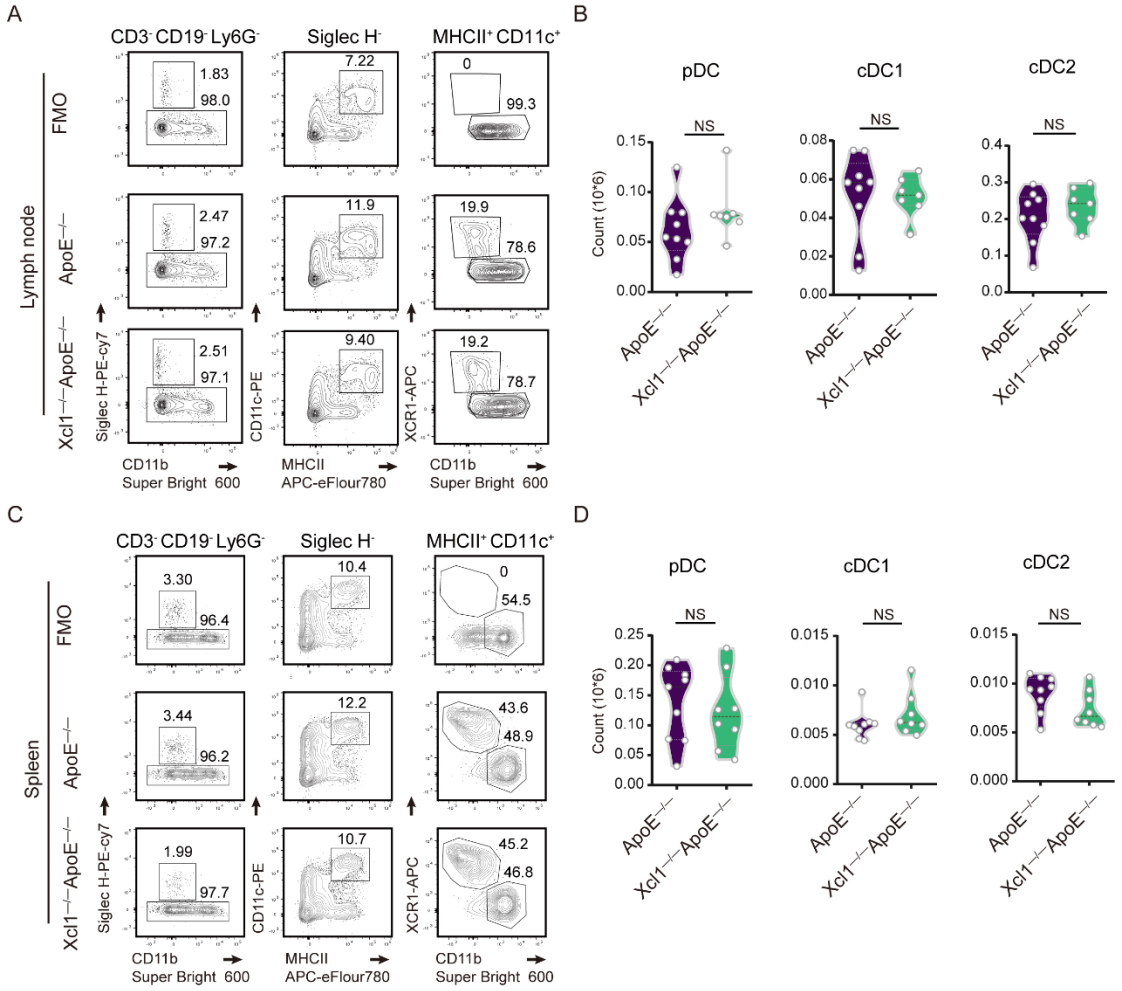
A
CD3⁻ CD19⁻ Ly6G⁻
Siglec H⁻
MHCII⁺ CD11c⁺
Lymph node
FMO
ApoE⁻/⁻
Xcl1⁻/⁻ApoE⁻/⁻
1.83
98.0
7.22
0
99.3
2.47
97.2
11.9
19.9
78.6
2.51
97.1
9.40
19.2
78.7
Siglec H-PE-cy7
CD11c-PE
XCR1-APC
CD11b Super Bright 600
MHCII APC-eFlour780
CD11b Super Bright 600
B
pDC
cDC1
cDC2
NS
Count (10^6)
ApoE⁻/⁻
Xcl1⁻/⁻ApoE⁻/⁻
C
Spleen
3.30
96.4
10.4
0
54.5
3.44
96.2
12.2
43.6
48.9
1.99
97.7
10.7
45.2
46.8
D

Figure S12

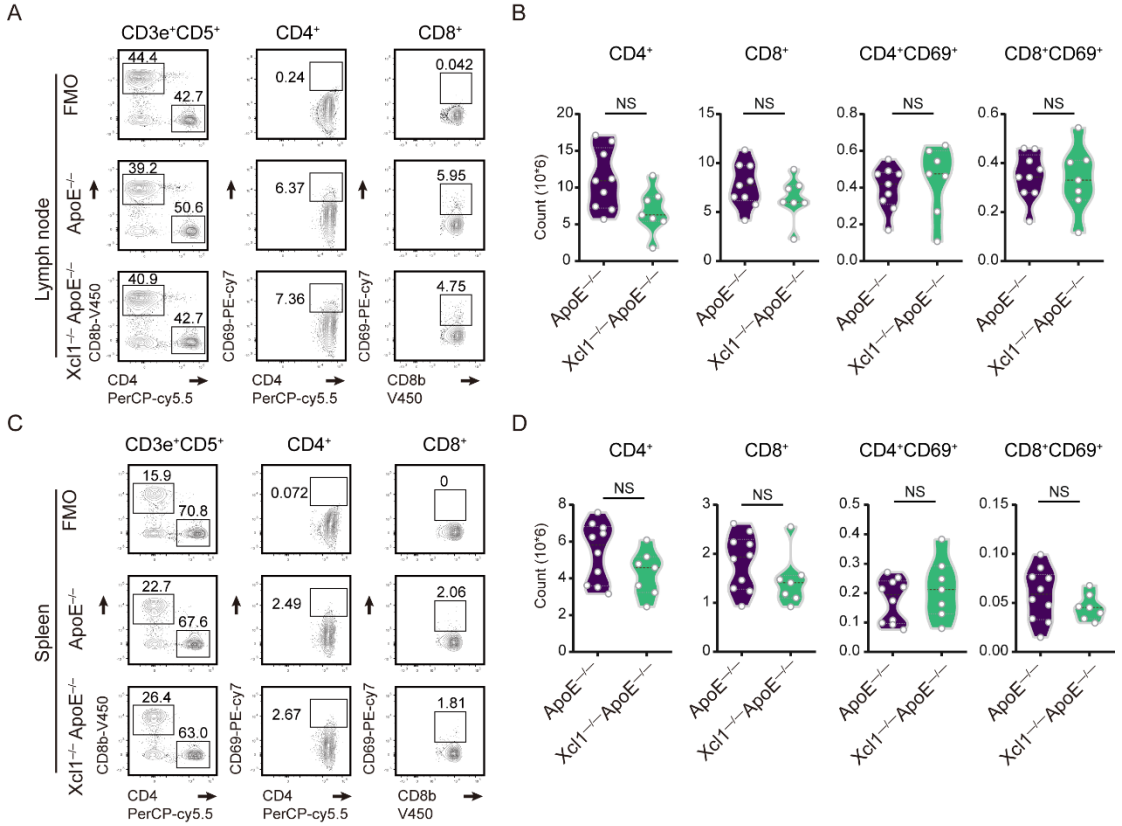
A
CD3e+CD5+
CD4+
CD8+
Lymph node
FMO
ApoE−/−
Xcl1−/− ApoE−/−
44.4
42.7
0.24
0.042
39.2
50.6
6.37
5.95
40.9
42.7
7.36
4.75
CD8b-V450
CD69-PE-cy7
CD4 PerCP-cy5.5
CD8b V450
B
CD4+
CD8+
CD4+CD69+
CD8+CD69+
NS
Count (10^6)
ApoE−/−
Xcl1−/− ApoE−/−
C
Spleen
15.9
70.8
0.072
0
22.7
67.6
2.49
2.06
26.4
63.0
2.67
1.81
D

Supplementary table 1

[GeneSet]

$SchemaVersion	1
$GeneSetName	Seurat Marker Features RunID: ZEE2
$GeneSetDescription	Generated in the Seurat analysis pipeline. Fold-Change > 5.2605272115588; q-Val (FDR) < 1

[Genes]	Log2 Fold-Change	q-Value	Cluster
Hspa1b	42.52120302	9.50E-177	1
Dnajb1	20.81074839	2.92E-90	1
Glrx	13.83830441	3.45E-48	1
Hes1	10.52069041	4.85E-44	1
Dnaja1	25.13842471	2.68E-41	1
Hspd1	12.1502349	7.64E-13	1
Lpar6	10.56634729	1.18E-11	1
Cxcr4	13.53264732	0.007875697	1
Cldnd1	33.56256056	1	1
Sat1	16.01666556	1	1
Stk17b	9.341881929	1.00E-120	2
Gpr171	8.036975348	6.90E-78	2
Cd36	37.33127974	3.01E-59	2
Plekho2	9.679954684	1.26E-51	2
Cd14	15.11839556	1.73E-20	2
Smim3	9.359129334	1.29E-10	2
Uck2	8.412740797	1.12E-09	2
Rraga	8.278727722	1.62E-06	2
Nsd1	8.142796627	8.74E-06	2
Sgk1	9.19132226	0.628752449	2
Ccl5	Inf	0	3
Epsti1	106.9899766	0	3
AW112010	37.55982075	0	3
Tspan3	29.08304265	0	3
Serpinb6b	43.04386652	2.81E-211	3
Vim	63.2513173	2.29E-95	3
Ccl22	178.6669207	6.38E-81	3
Tagln2	43.81517158	9.66E-79	3
Resf1	28.47128144	4.78E-63	3
Prdx1	34.18432187	4.61E-36	3
Slfn5	33.17542571	1.81E-130	4
Ifi44	11.07741437	1.18E-80	4
Irf7	18.03968574	4.53E-78	4
Stat1	11.19127012	2.20E-70	4

Ly6a	71.77936127	4.96E-35	4
Isg15	13.81873278	1.38E-27	4
Myd88	13.02295703	1.08E-11	4
Ifitm3	10.60216615	0.000403532	4
Nr4a2	12.68639324	1	4
Eprs	32.65659433	1	4
Ifrd1	13.16353946	7.56E-128	5
Nlrp3	14.45121644	2.01E-99	5
Tnfsf9	17.66324735	1.68E-76	5
Gpr65	23.75629403	3.36E-57	5
Itga4	14.48761702	1.91E-53	5
Aff1	15.6278723	6.96E-45	5
Lyz2	16.00040211	5.23E-30	5
Chd7	13.03464538	3.32E-27	5
Ccrl2	15.03814065	6.89E-19	5
Anxa1	17.1352024	0.000648149	5
Ube2c	34.35930797	0	6
Tuba1b	33.6015791	0	6
Hmgb2	21.96553285	0	6
Arl6ip1	20.79152855	0	6
Mki67	20.52766974	0	6
Tubb5	14.2678514	0	6
Cenpe	10.98235375	0	6
Top2a	19.59760586	2.19E-271	6
Cpox	12.47616675	3.47E-21	6
Hsph1	23.51902433	1	6
Fabp5	22.30871744	8.14E-283	7
2610528A11Rik	66.90179888	1.03E-218	7
S100a4	21.28583493	1.45E-149	7
Tmem123	69.90785515	4.20E-133	7
Mt1	52.98793574	4.91E-90	7
Gpr183	20.03728313	3.03E-84	7
S100a6	25.56962085	6.88E-76	7
Ctsc	23.64358551	2.62E-46	7
Cdk2ap2	39.81012543	9.71E-37	7
Clu	25.18396035	1.86E-20	7
Pcna	8.142821346	5.22E-182	8
Mcm7	5.358022282	3.65E-177	8
Mcm5	6.528065009	7.55E-166	8
Lig1	6.681288261	1.09E-157	8
Dut	5.260527212	6.64E-133	8
Paics	6.750359239	1.54E-111	8
Set	9.064414218	3.85E-87	8

Stmn1	6.753546782	8.71E-18	8
Tmem14c	7.079252859	1.11E-11	8
Npm3	7.295805042	1.78E-10	8
Nampt	14.01602029	5.52E-94	9
Serpina3g	21.08183631	2.44E-40	9
Sqstm1	35.71080346	2.69E-35	9
Nr4a3	46.8592915	2.27E-30	9
Prkcd	14.53860632	1.53E-28	9
Bcl2l11	16.47721576	2.90E-18	9
Cd274	20.28939966	4.91E-12	9
Ifi207	17.33536354	1.81E-09	9
Cdkn1a	14.73834176	6.97E-08	9
Gm19951	16.14302152	1.04E-06	9
Ets1	24.68664964	1.25E-263	10
Il2rb	40.60134549	3.11E-168	10
Nkg7	26.174639	5.46E-153	10
Xcl1	179.0903763	4.57E-147	10
Ighm	356.1167175	1.40E-138	10
Cd7	51.65059839	4.00E-68	10
Nrgn	63.22973626	6.64E-60	10
Igkc	Inf	1.11E-59	10
Ccnd2	22.7688043	1.11E-11	10
Odc1	79.11780903	1.83E-09	10

1074 **Supplementary table 2**

[GeneSet]				
$SchemaVersion	1			
$GeneSetName	up regulated genes in HFD-Aorta vs HFD-Spleen			
$GeneSetDescription				
[Genes]	fold_change(HFD-Aorta vs HFD-Spleen)	q-value(HFD-Aorta vs HFD-Spleen)	HFD-Aorta	HFD-Spleen
Ccr2	2.868	2.08E-13	2.7647	0.3127
Cldnd1	2.09622	4.98E-05	3.4706	1.1327
Ifi203	2.03954	0.000476302	1.5735	0.2618
Mndal	2.38451	4.03E-08	2.3677	0.4123
3-Sep	2.07201	2.26E-07	4.9706	1.8816
Wfdc17	2.01749	0.0194669	1.1765	0.0788

[GeneSet]				
$SchemaVersion	1			
$GeneSetName	up regulated genes in HFD-Aorta vs HFD-Lymph nodes			
$GeneSetDescription				
[Genes]	fold_change(HFD-Aorta vs HFD-Lymph nodes)	q-value(HFD-Aorta vs HFD-Lymph nodes)	HFD-Aorta	HFD-Lymph nodes
Ccr2	2.47261	2.08E-13	2.7647	0.5226
Cd24a	2.04889	1.39E-10	8.2206	3.5003
Ckb	2.43031	2.08E-13	4.2059	1.1421
Cldnd1	2.85069	2.08E-13	3.4706	0.5682
Cyth4	2.11238	2.08E-13	3.0588	0.9214
Dnaja1	3.22678	1.02E-10	6.7353	1.3972
Dnajb1	5.16719	2.48E-09	8.0735	0.756
Fgfr1	2.25182	2.08E-13	1.5441	0.1298
Hsp90aa1	4.50681	3.09E-08	21.441	3.9794
Hsp90ab1	2.13951	1.05E-05	29.074	13.056
Hspa1a	7.12033	2.08E-13	36.779	4.3059
Hspa1b	9.11898	2.08E-13	38.677	3.351
Hspa5	2.68952	2.39E-08	23.059	7.9454
Hspd1	2.33134	0.0275939	3.1471	0.7788
Hspe1	2.16981	1.12E-05	6.1029	2.2735
Hsph1	5.51596	1.10E-06	6.75	0.405
Ifitm2	2.29707	1.85E-11	3.3971	0.9142
Ifitm3	2.23302	0.000253682	2.0441	0.3632
Lyz2	2.1711	2.08E-13	4.0147	1.3098
Naaa	2.25383	2.08E-13	19.177	7.9521

Nr4a2	2.01215	0.0210806	2.5882	0.7833
Olfm1	2.03054	2.08E-13	4.2353	1.5783
Picalm	2.09067	8.77E-08	3.8382	1.3142
Plac8	2.56781	2.08E-13	4.8824	1.2908
Rac2	2.2199	2.08E-13	1.9706	0.3382
Rsrp1	2.13894	2.08E-13	3.3529	1.0351
3-Sep	2.06936	2.08E-13	4.9706	1.8852
Tiparp	2.05071	0.00113877	2.2206	0.5705
Wfdc17	2.08139	6.31E-06	1.1765	0.0457
Zfand2a	2.08069	0.040016	1.2059	0.0602

1077 **Supplementary table 3**

sgRNA		
sgRNA name	**sequence (5' > 3')**	**Purpose**
sgXcr1-KI	AGGCTGTAGAGGACTCCATC *TGG*	Generation of Xcr1$^{Cre\text{-}Gfp}$ knock-in mice
sgXcl1-1	TTGCGAGGGGCTTTCGGGGT *GGG*	Generation of *Xcl1* knockout mice
sgXcl1-2	CAAGCTGAACTTAAGAACGA *TGG*	

1078